Inorganic Chemistry

Article

pubs.acs.org/IC

Structural Diversities in Heterometallic Mn−Ca Cluster Chemistry from the Use of Salicylhydroxamic Acid: $\{Mn^{III}_4Ca_2\}$, $\{Mn^{II/III}_6Ca_2\}$, $\{Mn^{III/IV}_8Ca\}$, and $\{Mn^{III}_8Ca_2\}$ Complexes with Relevance to Both High- and Low-Valent States of the Oxygen-Evolving Complex

Alysha A. Alaimo,[†] Evangelia S. Koumousi,[‡] Luís Cunha-Silva,[§] Laura J. McCormick,[⊥] Simon J. Teat,[⊥] Vassilis Psycharis,[∥] Catherine P. Raptopoulou,[∥] Shreya Mukherjee,[¶] Chaoran Li,[¶] Sayak Das Gupta,[¶] Albert Escuer,[▽] George Christou,[¶] and Theocharis C. Stamatatos*[,†]

[†]Department of Chemistry, Brock University, 1812 Sir Isaac Brock Way, L2S 3A1 St. Catharines, Ontario, Canada

[‡]Department of Chemistry, University of Patras, 26504 Patras, Greece

[§]REQUIMTE-LAQV & Department of Chemistry and Biochemistry, Faculty of Sciences, University of Porto, 4169-007 Porto, Portugal

[⊥]Advanced Light Source, Lawrence Berkeley National Laboratory, 1 Cyclotron Road, Berkeley, California 94720, United States

[∥]Institute of Nanoscience and Nanotechnology, NCSR "Demokritos", 15310 Agia Paraskevi, Attikis, Greece

[¶]Department of Chemistry, University of Florida, Gainesville, Florida 32611-7200, United States

[▽]Departament de Quimica Inorganica and Institut de Nanociencia i Nanotecnologia (IN2UB), Universitat de Barcelona, Diagonal 645, 08028 Barcelona, Spain

Supporting Information

ABSTRACT: One-pot reactions between the $[Mn_3O(O_2CPh)_6(py)_x]^{+/0}$ triangular precursors and either $CaBr_2{\cdot}xH_2O$ or $CaCl_2{\cdot}6H_2O$, in the presence of salicylhydroxamic acid ($shaH_2$), have afforded the heterometallic complexes $[Mn^{III}_4Ca_2(O_2CPh)_4(shi)_4(H_2O)_3(Me_2CO)]$ (**1**) and $(pyH)[Mn^{II}_2Mn^{III}_4Ca_2Cl_2(O_2CPh)_7(shi)_4(py)_4]$ (**2**), respectively, in good yields. Further reactions but using a more flexible synthetic scheme comprising the $Mn(NO_3)_2{\cdot}4H_2O/Ca(NO_3)_2{\cdot}4H_2O$ and $Mn(O_2CPh)_2{\cdot}2H_2O/Ca(ClO_4)_2{\cdot}4H_2O$ "metal blends" and $shaH_2$, in the presence of external base NEt_3, led to the new complexes $(NHEt_3)_2[Mn^{III}_4Mn^{IV}_4Ca(OEt)_2(shi)_{10}(EtOH)_2]$ (**3**) and $(NHEt_3)_4[Mn^{III}_8Ca_2(CO_3)_4(shi)_8]$ (**4**), respectively. In all reported compounds, the anion of the tetradentate (N,O,O,O)-chelating/bridging ligand salicylhydroxime (shi^{3-}), resulting from the in situ metal-ion-assisted amide−iminol tautomerism of $shaH_2$, was found to bridge both Mn and Ca atoms. Complexes **1**−**4** exhibit a variety of different structures, metal stoichiometries, and Mn oxidation-state descriptions; **1** possesses an overall octahedral metal arrangement, **2** can be described as a Mn_4Ca_2 octahedron bound to an additional Mn_2 unit, **3** consists of a Mn_8 "ring" surrounding a Ca^{II} atom, and **4** adopts a rectangular cuboidal motif of eight Mn atoms accommodating two Ca^{II} atoms. Solid-state direct-current magnetic susceptibility studies revealed the presence of predominant antiferromagnetic exchange interactions between the Mn centers, leading to $S = 0$ spin ground-state values for all complexes. From a bioinorganic chemistry perspective, the reported compounds may demonstrate some relevance to both high-valent scheme (**3**) and lower-oxidation-level species (**1**, **2**, and **4**) of the catalytic cycle of the oxygen-evolving complex.

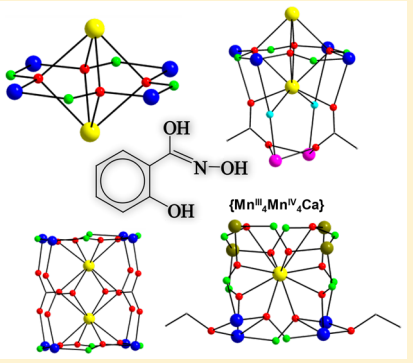

INTRODUCTION

The oxygen-evolving complex (OEC) of photosystem II (PSII) splits water into molecular O_2, protons, and electrons in green plants, algae, and cyanobacteria, generating the reducing equivalents and proton gradient that drive the rest of the photosynthetic process in the presence of sunlight.[1] Extensive research endeavors have been directed toward the synthesis of structural models (i.e., coordination compounds) that would potentially be able to mimic the structural and electronic properties of the inorganic core of OEC.[2] This would subsequently allow scientists to gain insight into the properties and function of the biological catalyst, as well as to understand and correlate the structural role of several components (i.e., metal ions, ligands, etc.) with the activity of the native enzyme itself toward the development of artificial photosynthesis.[3]

The OEC contains a heterometallic $\{Mn_4CaO_5\}$ cluster (Scheme 1),[4] also known as the water-oxidizing complex

Received: July 8, 2017
Published: August 17, 2017

DOI: 10.1021/acs.inorgchem.7b01740
Inorg. Chem. 2017, 56, 10760−10774

Scheme 1. Latest Model for the $\{Mn_4CaO_5\}$ Cluster of the OEC Core in PSII

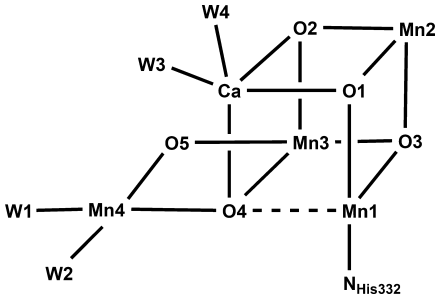

(WOC), which consists of an oxido-bridged $\{Mn_3CaO_4\}$ distorted cubane unit linked to a fourth, dangling Mn atom through one of the unit's oxido bridges and an additional bis-μ-O^{2-} group (O5; Scheme 1). Peripheral ligation about the overall $\{Mn_4CaO_5\}$ core is mostly provided by aspartate and glutamate carboxylate groups of various polypeptide moieties, as well as one histidine (N_{His332}) and four H_2O molecules or water-derived ligands (W1–W4; Scheme 1).[5] X-ray absorption spectroscopy, including extended X-ray absorption fine structure and X-ray absorption near-edge spectroscopy, has been an invaluable tool in assessing the metal topology, stoichiometry, and distances between atoms that compose the OEC.[6] These studies, along with electron paramagnetic resonance (EPR) spectroscopy,[7] have allowed for the description of the Mn oxidation states at each of the S states (S_n, where n = 0–4) of the catalytic Kok cycle, where the subscript indicates the number of stored oxidizing equivalents.[8] The Mn ions at the various S_n Kok states exist in high oxidation states and are described as a mixture of Mn^{III}, Mn^{IV}, and probably Mn^{V}.[1,2,9] The S_0 state is $3Mn^{III}/Mn^{IV}$, the dark-stable S_1 state is $2Mn^{III}/2Mn^{IV}$, the S_2, which is probably the most studied Kok state, is $Mn^{III}/3Mn^{IV}$, the metastable S_3 state has a $4Mn^{IV}$ or $Mn^{III}/3Mn^{IV}$-ligand radical description, and the transient S_4 state is either a $4Mn^{IV}$-ligand radical description or $3Mn^{IV}/Mn^{V}$.[10] During the fourth oxidation, O_2 is evolved, and the catalyst is reset to the S_0 state. In addition, the presence of the Ca^{II} atom is very important for the activity of the OEC; without its existence, the OEC could not advance to the metastable S_3 state.[11] The substitution of other metal ions for Ca^{II} leads to inhibition of the catalytic activity, except for Sr^{II}, which partially recovers activity.[12] Furthermore, the first atomic-resolution (1.9 Å) model of the native OEC by Umena and co-workers[13] revealed the presence of two Cl^- atoms in the vicinity of the $\{Mn_4Ca\}$ cluster, as well as one bicarbonate ion in close proximity. These anions have mainly a structural role, and they serve to stabilize the catalytic center of the OEC. In contrast, the coordinated oxido groups appear to have a more crucial role in the stabilization of the high Mn oxidation states, the satisfaction of the Ca^{II} oxophilicity, and eventually the assembly of the five metal ions into the extended, distorted cubane topology of the OEC.[14] Oxides are usually generated from the complete deprotonation of H_2O molecules; the process by which the OEC is assembled, called photoactivation, utilizes Mn, Ca, Cl^-, H_2O, and oxidizing equivalents resulting from light absorption.[15]

The determination of kinetically distinct species during the photoactivation process and the reduction of the S_n intermediates in the Kok cycle have led to species in oxidation states lower than S_0, which do not require the presence of oxido groups;[16] these S_n states (n = 1–, 2–, 3–) are known as the reduced OEC states and contain Mn ions in lower oxidation states (i.e., Mn^{II}, Mn^{III}).[17] During the catalytic turnover, lower-oxidation-state species with lower O-atom content must be generated upon the loss of molecular O_2.[18] The ligand set environment is then responsible for the periodic reorganization, reoxidation, and reoxygenation of the $\{Mn_4CaO_x\}$ cluster.[19] Therefore, the synthesis and detailed study of synthetic analogues of the OEC containing Mn ions in the 2+/3+ oxidation states would also be interesting and would greatly enhance our understanding of the spectroscopic, physical, and catalytic properties of the WOC, as well as its reactivity and functional characteristics.

Although multinuclear, homometallic Mn clusters at various oxidation-state levels and descriptions have been extensively reported over the last 2 decades or so,[20] heterometallic Mn–Ca molecular cluster chemistry has been only sparingly developed.[21] Agapie and co-workers,[22] Zhang and co-workers,[23] and a few of us[24] have reported some of the closest structural models to the native OEC core, all containing the desired $\{Mn_3CaO_4\}$ cubane core and Mn atoms in high oxidation states (i.e., Mn^{IV}). In all cases, different chelating and bridging ligands have been utilized, including carboxylates and pyridyl polyalcohols, among others. These molecular compounds nicely resemble some of the latter S states (S_2 and S_3) of the catalytic Kok cycle within the native OEC. Along these lines, Pantazis and co-workers have recently reviewed the individual or combined synthetic targets for the structural biomimetic chemistry of the OEC.[25]

We have recently started a program aimed at the exploration of the low oxidation states (S_n states; n = 1–, 2–, 3–) of the catalytic cycle through the synthesis of heterometallic Mn–Ca complexes with unique structural motifs, diverse topologies, and different Mn oxidation-state descriptions that would not require their stabilization and crystallization to occur in the presence of bridging oxido groups.[26] Following up with the elegant work of Pecoraro and co-workers in 3d and 3d/4f-metal chemistry,[27] we have also shown that salicylhydroxamic acid ($shaH_2$; Scheme 2), a photosynthetically effective group,[28] can

Scheme 2. Metal-Assisted Amide–Iminol Tautomerism of $shaH_2$ to $shiH_3$

$shaH_2$ **$shiH_3$**

undergo a metal-assisted amide–iminol tautomerism, which leads to the ligand salicylhydroxime ($shiH_3$; Scheme 2). The latter is an oximate-based ligand with four coordination sites available for binding to both Mn and Ca metal centers. The employment of $shiH_3$ in Mn–Ca chemistry has previously led us to the synthesis of the first family of oxido-free $\{Mn^{III}_4Ca\}$ complexes with a square-pyramidal topology and the exact metal stoichiometry as that found in the native OEC.[26] In this work, we have discovered new synthetic conditions to unveil four different heterometallic Mn–Ca/shi^{3-} complexes with diverse nuclearities, metal stoichiometries, and oxidation-state descriptions of relevance to both high and low oxidation states

DOI: 10.1021/acs.inorgchem.7b01740
Inorg. Chem. 2017, 56, 10760–10774

of the OEC. The synthesis, structures, and magnetic properties of the heterometallic $\{Mn^{III}_4Ca_2\}$, $\{Mn^{II/III}_6Ca_2\}$, $\{Mn^{III/IV}_8Ca\}$, and $\{Mn^{III}_8Ca_2\}$ complexes are reported herein.

EXPERIMENTAL SECTION

Synthesis. All manipulations were performed under aerobic conditions using chemicals and solvents as received, unless otherwise stated. The starting materials $Mn(O_2CPh)_2{\cdot}2H_2O$, $[Mn_3O(O_2CPh)_6(py)_3](ClO_4)$, and $[Mn_3O(O_2CPh)_6(py)_2(H_2O)]$ (py = pyridine) were prepared as described elsewhere.[29] ***Caution!*** *Perchlorate salts are potentially explosive; such compounds should be synthesized and used in small quantities and treated with the utmost care at all times.*

*$[Mn_4Ca_2(O_2CPh)_4(shi)_4(H_2O)_3(Me_2CO)]$ (**1**).* To a stirred, colorless solution of $shaH_2$ (0.31 g, 2.0 mmol) in Me_2CO (30 mL) were added the solids $[Mn_3O(O_2CPh)_6(py)_3](ClO_4)$ (0.87 g, 0.7 mmol) and $CaBr_2{\cdot}xH_2O$ (0.20 g, 1.0 mmol). The resulting brown suspension was stirred for 1 h, during which time all of the solids dissolved, and the color of the solution changed to dark brown. The solution was filtered and left to evaporate slowly at room temperature. After 5 days, brown platelike crystals of $\mathbf{1}{\cdot}3Me_2CO{\cdot}2.8H_2O$ appeared and were collected by filtration, washed with Me_2CO (2 × 5 mL) and Et_2O (2 × 5 mL), and dried in air; the yield was 60%. The crystalline solid was analyzed as $\mathbf{1}{\cdot}2H_2O$: C, 46.23; H, 3.42; N, 3.65. Found: C, 46.43; H, 3.58; N, 3.54. Selected attenuated total reflectance (ATR) data (cm^{-1}): 3058 (wb), 1595 (s), 1567 (s), 1543 (m), 1509 (s), 1432 (m), 1389 (vs), 1316 (s), 1244 (m), 1157 (m), 1100 (m), 1068 (w), 1023 (m), 929 (s), 864 (w), 838 (w), 749 (w), 721 (vs), 678 (vs), 648 (s), 602 (vs), 531 (w), 477 (s), 408 (m).

*$(pyH)[Mn_6Ca_2Cl_2(O_2CPh)_7(shi)_4(py)_4]$ (**2**).* To a stirred, colorless suspension of $shaH_2$ (0.08 g, 0.5 mmol) in CH_2Cl_2 (30 mL) were added the solids $[Mn_3O(O_2CPh)_6(py)_2(H_2O)]$ (0.54 g, 0.5 mmol) and $CaCl_2{\cdot}6H_2O$ (0.11 g, 0.5 mmol). The resulting red suspension was stirred for 2 h, during which time all of the solids dissolved, and the color of the solution changed to brown. The solution was filtered, and Et_2O (60 mL) diffused into the filtrate. After 10 days, red rodlike crystals of $\mathbf{2}{\cdot}2Et_2O{\cdot}CH_2Cl_2$ appeared and were collected by filtration, washed with CH_2Cl_2 (2 × 5 mL) and Et_2O (2 × 5 mL), and dried in air; the yield was 45%. The crystalline solid was analyzed as solvent-free **2**: C, 52.68; H, 3.34; N, 5.42. Found: C, 52.59; H, 3.25; N, 5.64. Selected ATR data (cm^{-1}): 3041 (m), 1597 (s), 1569 (s), 1512 (m), 1487 (m), 1468 (m), 1445 (m), 1432 (m), 1393 (vs), 1359 (s), 1319 (s), 1250 (m), 1218 (m), 1176 (m), 1099 (m), 1067 (m), 1037 (s), 927 (s), 865 (s), 838 (m), 754 (m), 719 (vs), 672 (vs), 647 (s), 475 (vs), 434 (m).

*$(NHEt_3)_2[Mn_8Ca(OEt)_2(shi)_{10}(EtOH)_2]$ (**3**).* To a stirred, colorless solution of $shaH_2$ (0.08 g, 0.5 mmol) and NEt_3 (0.21 mL, 1.5 mmol) in EtOH (30 mL) were added the solids $Mn(NO_3)_2{\cdot}4H_2O$ (0.13 g, 0.5 mmol) and $Ca(NO_3)_2{\cdot}4H_2O$ (0.12 g, 0.5 mmol). The resulting dark-red suspension was stirred for 1 h, during which time all of the solids dissolved, and the color of the solution changed to very dark brown. The solution was filtered and left to evaporate slowly at room temperature. After 2 weeks, dark-brown platelike crystals of $\mathbf{3}{\cdot}3EtOH{\cdot}H_2O$ appeared and were collected by filtration, washed with cold EtOH (2 × 5 mL) and Et_2O (2 × 5 mL), and dried in air; the yield was 30%. The crystalline solid was analyzed as $\mathbf{3}{\cdot}2H_2O$: C, 43.86; H, 4.19; N, 7.14. Found: C, 43.71; H, 4.12; N, 7.22. Selected ATR data (cm^{-1}): 3375 (mb), 3062 (m), 2966 (mb), 1595 (s), 1564 (s), 1471 (vs), 1384 (vs), 1314 (vs), 1257 (s), 1153 (m), 1098 (m), 1034 (s), 950 (s), 860 (s), 752 (s), 672 (vs), 641 (s), 591 (sb), 461 (m).

*$(NHEt_3)_4[Mn_8Ca_2(CO_3)_4(shi)_8]$ (**4**).* To a stirred, colorless solution of $shaH_2$ (0.08 g, 0.5 mmol) and NEt_3 (0.21 mL, 1.5 mmol) in $CHCl_3$ (30 mL) were added the solids $Mn(O_2CPh)_2{\cdot}2H_2O$ (0.17 g, 0.5 mmol) and $Ca(ClO_4)_2{\cdot}4H_2O$ (0.16 g, 0.5 mmol). The resulting dark-red suspension was stirred for 3 h, during which time all of the solids dissolved, and the color of the solution changed to dark brown. The solution was filtered and left to evaporate slowly at room temperature. After 1 month, brown platelike crystals of $\mathbf{4}{\cdot}9CHCl_3$ appeared and were collected by filtration, washed with $CHCl_3$ (2 × 5 mL) and Et_2O (2 × 5 mL), and dried under vacuum; the yield was 20%. The crystalline solid was analyzed as $\mathbf{4}{\cdot}2CHCl_3$: C, 40.22; H, 3.85; N, 6.54. Found: C, 40.36; H, 3.99; N, 6.48. Selected ATR data (cm^{-1}): 2993 (mb), 1595 (s), 1566 (s), 1508 (s), 1468 (m), 1448 (m), 1432 (s), 1375 (vs), 1316 (s), 1255 (s), 1155 (m), 1098 (m), 1066 (m), 1027 (s), 935 (s), 863 (s), 749 (vs), 720 (vs), 673 (vs), 645 (vs), 609 (vs), 532 (m), 443 (s), 415 (m).

X-ray Crystallography. A brown single crystal of complex $\mathbf{1}{\cdot}3Me_2CO{\cdot}2.8H_2O$ was mounted in a capillary with drops of mother liquid because they were destroyed immediately when immersed in the crystallographic oil; this was confirmed by the presence of many partially occupied solvate molecules. Diffraction measurements were made at room temperature on a Rigaku R-AXIS SPIDER image-plate diffractometer using graphite-monochromated Cu Kα radiation. Data collection (ω scans) and processing (cell refinement, data reduction, and empirical absorption correction) were performed using the *CrystalClear* program package.[30] The structure was solved by direct methods using *SHELXS-97*[31,38] and refined by full-matrix least-squares techniques on F^2 with *SHELXL*, version 2014/6.[32] All non-H atoms were refined anisotropically, except from those belonging to partially occupied solvate molecules, which were refined isotropically. All H atoms were introduced at calculated positions as riding on their respective atoms. No H atoms for the partially occupied solvate molecules were included in the refinement. The O2W and O41 atoms that belong to the coordinated H_2O and acetone molecules are disordered with site occupancies of 0.5.

Data for complexes $\mathbf{2}{\cdot}2Et_2O{\cdot}CH_2Cl_2$ and $\mathbf{3}{\cdot}3EtOH{\cdot}H_2O$ were collected on a beamline 11.3.1 at the Advanced Light Source, Lawrence Berkeley National Laboratory. Samples were mounted on MiTeGen kapton loops and placed in a 100(2) K cold nitrogen stream provided by an Oxford Cryostream 700 Plus low-temperature apparatus on the goniometer head of a Bruker D8 diffractometer equipped with a PHOTON100 CMOS detector operating in shutterless mode. Diffraction data were collected using monochromated synchrotron radiation [silicon(111) to wavelengths of 0.8856(1) and 0.7749(1) Å for **2** and **3**, respectively]. An approximate full sphere of data was collected using a combination of ϕ and ω scans with scan speeds of 1 s/4° for the ϕ scans, and 1 and 3 s/deg for the ω scans at $2\theta = 0$ and −45°, respectively. The structures were solved by intrinsic phasing (*SHELXT*) and refined by full-matrix least squares on F^2 (*SHELXL-2014*). All non-H atoms were refined anisotropically. H atoms were geometrically calculated and refined as riding atoms. For complex **2**, the coordinated pyridine molecules were found to be disordered and the C atoms have been modeled over two sites with complementary occupancies. Some minor rotational disorder was also found for the aromatic rings of the shi^{3-} and $PhCO_2^-$ groups. The free pyridinium cation is rotationally disordered over two sites, such that the −NH group can occupy one of the two symmetry-related sites. The C and N atoms that occupy this site have been refined with an occupancy of 0.5, with the same *xyz* coordinates and isotropic displacement parameters as each other. The partial occupancy of the CH_2Cl_2 molecule was found to be disordered over two symmetry-related sites, and the atoms were refined isotropically with a site occupancy of 0.5. The C3E−C4E ethyl chain of the Et_2O molecule was found to be disordered; however, only the major orientation of this chain could be modeled satisfactorily (occupancy of 0.81). For complex **3**, all non-H atoms belonging to the cluster were located. The aromatic ring of one shi^{3-} ligand was found to be disordered and has been modeled over two sites with complementary site occupancies. In addition to the cluster compound, there are two triethylammonium ($NHEt_3^+$) cations, three guest EtOH molecules, and a H_2O molecule. The two $NHEt_3^+$ cations were found to be disordered and have been modeled over two locations. Similarly, the EtOH molecules were each found to be disordered and have been modeled over two or three different positions. Equivalent atoms have been constrained to have equal U_{ij} values. Different orientations of the same molecule have been restrained to have equal bond lengths and angles by using the RESI and SAME commands. The ammonium H atom belonging to the minor orientation of the N1a cation has been held in place using SDAI commands and keeping an equal distance between the H atom and three C atoms bound to the central N atom. All ammonium and

DOI: 10.1021/acs.inorgchem.7b01740
Inorg. Chem. 2017, 56, 10760−10774

Table 1. Crystallographic Data for Complexes 1−4

	1·3Me$_2$CO·2.8H$_2$O	**2**·2Et$_2$O·CH$_2$Cl$_2$	**3**·3EtOH·H$_2$O	**4**·9CHCl$_3$
empirical formula[a]	$C_{68}H_{71.6}Mn_4Ca_2N_4O_{29.8}$	$C_{111}H_{100}Mn_6Ca_2N_9O_{28.5}Cl_4$	$C_{93.88}H_{107.62}Mn_8CaN_{12}O_{36.94}$	$C_{93}H_{105}Mn_8Ca_2N_{12}O_{36}Cl_{27}$
fw[a]/g mol^{-1}	1721.61	2567.59	2474.64	3443.71
cryst type	brown plate	red rod	dark-brown plate	brown plate
cryst size/mm	0.28 × 0.49 × 0.80	0.20 × 0.04 × 0.04	0.08 × 0.07 × 0.06	0.16 × 0.16 × 0.08
cryst syst	monoclinic	orthorhombic	orthorhombic	monoclinic
space group	*C*2/*c*	*Pnna*	*Pbca*	*P*2$_1$/*c*
a/Å	26.9129(5)	20.4296(8)	19.897(2)	17.0486(7)
b/Å	14.1766(3)	24.9250(10)	21.418(2)	20.8611(8)
c/Å	24.1414(4)	21.6928(8)	47.738(5)	21.1323(8)
α/deg	90	90	90	90
β/deg	92.403(1)	90	90	111.309(2)
γ/deg	90	90	90	90
V/Å^3	9202.7(3)	11046.1(7)	20344(4)	7001.9(5)
Z	4	4	8	2
T/K	293	100.0(2)	100.0(2)	150(2)
ρ_{calc}/g cm^{-3}	1.243	1.544	1.616	1.633
μ/mm^{-1}	5.951	1.705	1.388	1.359
θ range/deg	6.60−64.99	2.34−39.33	2.63−29.42	3.65−25.03
index ranges	$-31 \le h \le 31$, $-13 \le k \le 16$, $-28 \le l \le 28$	$-29 \le h \le 29$, $-35 \le k \le 35$, $-31 \le l \le 31$	$-25 \le h \le 25$, $-26 \le k \le 27$, $-60 \le l \le 60$	$-20 \le h \le 20$, $-24 \le k \le 24$, $-25 \le l \le 25$
collcd reflns	44128	245372	171165	88540
indep reflns	7680 (R_{int} = 0.0732)	16916 (R_{int} = 0.0507)	21624 (R_{int} = 0.0928)	7805 (R_{int} = 0.0831)
final R[b] indices [$I > 2\sigma(I)$]	R1 = 0.0711, wR2 = 0.2008[c]	R1 = 0.0735, wR2 = 0.1932	R1 = 0.0547, wR2 = 0.1321	R1 = 0.1351, wR2 = 0.3940
$(\Delta\rho)_{max,min}$/e Å^{-3}	0.668, −0.513	1.427, −1.363	0.977, −0.562	5.790, −1.591

[a]Including solvate molecules. [b]R1 = $\sum(||F_o| - |F_c||)/\sum|F_o|$. wR2 = $[\sum[w(F_o^2 - F_c^2)^2]/\sum[w(F_o^2)^2]]^{1/2}$, with $w = 1/[\sigma^2(F_o^2) + (ap)^2 + bp]$, where $p = [\max(F_o^2,0) + 2F_c^2]/3$. [c]For 5879 reflections with $I > 2\sigma(I)$.

hydroxido H atoms were located at the difference map, fixed at distances of 0.88 and 0.84 Å from the N or O atoms, respectively, to which they are bound, and given a thermal displacement parameter of 1.2 or 1.5 times that of the corresponding N or O atom to which they are bound. Not all hydroxido or water H atoms could be located during the refinement. These "missing" H atoms have been included in the molecular formula but not in the final model.

A selected crystal of complex **4**·9CHCl$_3$ was manually harvested and mounted on a cryoloop using adequate oil.[33] All of the single crystals chosen for data collection showed very weak X-ray diffraction patterns under the accessible Mo Kα radiation. It was not feasible to obtain any better diffraction for this complex, but the reported data are of good enough quality to adequately confirm the metals' connectivity and most of the molecules in the crystal lattice. Diffraction data were collected at 150.0(2) K on a Bruker X8 Kappa APEX II charge-coupled-device area-detector diffractometer controlled by the *APEX2* software package[34] (graphite-monochromated Mo Kα radiation, λ = 0.71073 Å) and equipped with an Oxford Cryosystems series 700 cryostream monitored remotely with the software interface *Cryopad*.[35] Images were processed with the software *SAINT+*,[36] and absorption effects were corrected with the multiscan method implemented in *SADABS*.[37] The structure was solved using the algorithm implemented in *SHELXT-2014*[38,39] and refined by successive full-matrix least-squares cycles on F^2 using the latest *SHELXL-v.2014*.[38,40] The non-H atoms were successfully refined using anisotropic displacement parameters. H atoms bonded to C atoms were placed at their idealized positions using the appropriate HFIX instructions in *SHELXL* and included in subsequent refinement cycles in a riding-motion approximation with isotropic thermal displacement parameters (U_{iso}) fixed at 1.2 or 1.5U_{eq} of the relative atom. Considerable electron density was found on the data of the crystal structure, probably because of additional disordered solvate molecules occupying the spaces created by the packing arrangement of the complexes. Efforts to accurately locate, model, and refine these residues turned out to be ineffective, and the investigation for the total potential solvent area using the software package *PLATON*[41a,b] confirmed the existence of cavities with potential solvent-accessible void volume. Thus, the original data sets were treated with the program *SQUEEZE*,[41c] which calculates the contribution of the smeared electron density in the lattice voids and adds this to the calculated structure factors from the structural model upon refinement against the *hkl* file.

The programs used for molecular graphics were *MERCURY*[41d] and *DIAMOND*.[41e] Unit cell parameters and structure solution and refinement data for all complexes are listed in Table 1. Crystallographic data (excluding structure factors) for the structures reported in this work have been deposited to the Cambridge Crystallographic Data Centre (CCDC) as supplementary publication numbers CCDC 1559579 (**1**·3Me$_2$CO·2.8H$_2$O), 1559399 (**2**·2Et$_2$O·CH$_2$Cl$_2$), 1559398 (**3**·3EtOH·H$_2$O), and 1559957 (**4**·9CHCl$_3$).

Physical Measurements. IR spectra were recorded in the solid state on a Bruker Fourier transform infrared spectrometer (ALPHA's Platinum ATR single reflection) in the 4000−400 cm^{-1} range. Elemental analyses (C, H, and N) were performed on a PerkinElmer 2400 series II analyzer. Magnetic susceptibility studies were performed at the Chemistry Department, University of Florida, on a Quantum Design MPMS-XL SQUID susceptometer equipped with a 7 T magnet and operating in the 1.8−400 K range. Samples were embedded in solid eicosane to prevent torquing. Pascal's constants were used to estimate the diamagnetic correction, which was subtracted from the experimental susceptibility to give the molar paramagnetic susceptibility (χ_M).[42]

RESULTS AND DISCUSSION

Synthesis and IR Spectra. Two different synthetic strategies were employed for the synthesis and crystallization of the reported heterometallic Mn−Ca cluster compounds. The first utilizes either the charged $[Mn_3O(O_2CPh)_6(py)_3]^+$ triangle as the starting material, which comprises three Mn^{III} atoms, or the mixed-valence, neutral $[Mn_3O(O_2CPh)_6(py)_2(H_2O)]$ triangle (2Mn^{III} and 1Mn^{II}), in the presence of CaX_2 sources [X$^-$ = halides; Br (for **1**) and Cl (for **2**)] and shaH$_2$. In this first

DOI: 10.1021/acs.inorgchem.7b01740
Inorg. Chem. 2017, 56, 10760−10774

route, no external organic base was used because the role of the proton acceptor could be undertaken by the carboxylate groups, pyridine molecules, and/or oxido ions of the $\{Mn_3\}$ starting materials. The oxide-centered and carboxylate-bridged $\{Mn_3\}$ triangles have been proven to be invaluable sources for the synthesis of high-nuclearity, homometallic $\{Mn_x\}$ clusters of various large nuclearities and high oxidation states for the metal atoms.[43] The second route that was followed includes the reactions between simpler, monomeric Mn^{II}- and Ca^{II}-containing starting materials in the presence of the chelating/bridging organic ligand $shaH_2$ and base NEt_3. The latter was used to facilitate deprotonation of the $shaH_2/shiH_3$ ligands and subsequently generate $NHEt_3^+$ cations in solution, which can potentially counterbalance the anionic charge of a cluster compound in solution and help with crystallization of the resulting salt in the solid state. Finally, various solvents and metal/$shaH_2$ ratios were explored to target crystallization of the reported molecular compounds.

Therefore, the one-pot reaction of $[Mn_3O(O_2CPh)_6(py)_3](ClO_4)$ and $CaBr_2\cdot xH_2O$ with $shaH_2$ in a 1:1.5:3 molar ratio in Me_2CO gave a dark-brown solution that, upon filtration and slow evaporation at room temperature, afforded brown crystals of the complex $[Mn^{III}_4Ca_2(O_2CPh)_4(shi)_4(H_2O)_3(Me_2CO)]$ (**1**) in 60% yield (based on the total available Ca). A reaction similar to that of **1**, albeit with $[Mn_3O(O_2CPh)_6(py)_2(H_2O)]$ and $CaCl_2\cdot 6H_2O$ in the presence of $shaH_2$, in a molar ratio of 1:1:1 and in the solvent CH_2Cl_2, led to a brown solution that, upon filtration and slow diffusion with Et_2O, afforded red crystals of a new, mixed-valence complex, $(pyH)[Mn^{II}_2Mn^{III}_4Ca_2Cl_2(O_2CPh)_7(shi)_4(py)_4]$ (**2**), in 45% yield (based on the total available Ca). The formation of complexes **1** and **2** is summarized in the balanced eqs 1 and 2, respectively.

$$\begin{aligned} &4[Mn_3O(O_2CPh)_6(py)_3](ClO_4) + 6CaBr_2 + 12shiH_3 \\ &\quad + 5H_2O + 3Me_2CO \\ &\rightarrow 3[Mn_4Ca_2(O_2CPh)_4(shi)_4(H_2O)_3(Me_2CO)] \\ &\quad + 12PhCO_2H + 12(pyH)Br + 4HClO_4 \end{aligned} \quad (1)$$

$$\begin{aligned} &2[Mn_3O(O_2CPh)_6(py)_2(H_2O)] + 2CaCl_2\cdot 6H_2O \\ &\quad + 4shiH_3 + py \\ &\rightarrow (pyH)[Mn_6Ca_2Cl_2(O_2CPh)_7(shi)_4(py)_4] \\ &\quad + 5PhCO_2H + 2HCl + 16H_2O \end{aligned} \quad (2)$$

Analogous reactions with different carboxylate-based $\{Mn_3\}$ triangles as starting materials (i.e., acetates, propionates, pivalates, etc.) all failed to yield single crystals suitable for X-ray diffraction studies. We have thus turned our synthetic endeavors toward one-pot reactions between $Mn(NO_3)_2\cdot 4H_2O$, $Ca(NO_3)_2\cdot 4H_2O$, $shaH_2$, and NEt_3 in various molar ratios and solvents. Only from the 1:1:1:3 reaction of the aforementioned precursors in the solvent EtOH we were able to grow dark-brown crystals of a nonanuclear, mixed-valence complex, $(NHEt_3)_2[Mn^{III}_4Mn^{IV}_4Ca(OEt)_2(shi)_{10}(EtOH)_2]$ (**3**), in 30% yield (based on the total available Ca). It becomes apparent that the reaction solvent has an important role in the synthesis and crystallization of **3**; both bridging EtO^- groups and terminally bound EtOH molecules were found in the structure of **3** (vide infra). Reactions in different alcohols did not yield any crystalline materials but only amorphous precipitates that we were unable to redissolve and crystallize.

Expanding this synthetic protocol further, we decided to perform the 1:1:1:3 reaction between $Mn(O_2CPh)_2\cdot 2H_2O$, $Ca(ClO_4)_2\cdot 4H_2O$, $shaH_2$, and NEt_3 in the solvent $CHCl_3$. The resulting brown solution was left to evaporate slowly at room temperature and, over a period of approximately 1 month, brown crystals formed in yields as high as 20%, which turned out to be a new decanuclear complex, $(NHEt_3)_4[Mn^{III}_8Ca_2(CO_3)_4(shi)_8]$ (**4**). The coordinated CO_3^{2-} ions (vide infra) were presumably derived from the fixation of atmospheric CO_2 during aerobic reactions.[44] This could also explain the prolonged crystallization period of **4** compared to the other compounds **1**−**3**. The formation of complexes **3** and **4** is summarized in the balanced eqs 3 and 4, respectively.

$$\begin{aligned} &8Mn(NO_3)_2\cdot 4H_2O + Ca(NO_3)_2\cdot 4H_2O + 10shiH_3 + 3O_2 \\ &\quad + 20NEt_3 + 4EtOH \\ &\rightarrow (NHEt_3)_2[Mn_8Ca(OEt)_2(shi)_{10}(EtOH)_2] \\ &\quad + 18(NHEt_3)(NO_3) + 42H_2O \end{aligned} \quad (3)$$

$$\begin{aligned} &8Mn(O_2CPh)_2\cdot 2H_2O + 2Ca(ClO_4)_2\cdot 4H_2O + 8shiH_3 \\ &\quad + 2O_2 + 24NEt_3 + 4CO_2 \\ &\rightarrow (NHEt_3)_4[Mn_8Ca_2(CO_3)_4(shi)_8] + 16(NHEt_3) \\ &\quad (O_2CPh) + 4(NHEt_3)(ClO_4) + 24H_2O \end{aligned} \quad (4)$$

The reactions that gave **3** and **4** are both oxidations, undoubtedly by O_2 under the prevailing basic conditions. None of the anions accompanying the metal ions' starting materials appear to participate in the molecular structures of **3** and **4**. NEt_3 has the role of proton acceptor to facilitate deprotonation of the $shiH_3$ groups and solvate molecules (i.e., EtOH to EtO^-). In addition, both anionic clusters **3** and **4** are stabilized by $NHEt_3^+$ countercations. Employment of different organic bases, such as NMe_3, Bu^n_3N, and Me_4NOH, did not afford crystalline materials but only oily products that we were not able to further characterize. In all complexes **1**−**4**, the coordinated shi^{3-} groups resulted from the metal-ion-assisted transformation of $shaH_2$ under the reported synthetic conditions (vide infra). Finally, by adjusting the experimental molar ratios of the precursors to the stoichiometric equivalents in an attempt to optimize the isolated yields, we failed to reproduce the crystals of all reported complexes.

Unfortunately, complexes **1**−**4** do not appear to retain their solid-state structures in solutions of various solvent media (i.e., MeCN, CH_2Cl_2, and THF), as it was confirmed by electrospray ionization mass spectrometry. It is very possible that this diversity of species in solution is one of the main reasons for crystallizing and structurally characterizing in the solid-state four different compounds from the Mn−Ca/$shaH_2$ reaction system. We have thus concentrated on the solid-state characterization of these species, which includes IR spectroscopy and magnetic susceptibility studies. All complexes **1**−**4** have similar IR spectra that are dominated by the stretching vibrations of the aromatic rings of shi^{3-} in the ∼1595−1380 cm^{-1} range; these bands in complexes **1** and **2** overlap with stretches from the carboxylate groups, thus rendering their exact assignments very difficult.[45] Contributions from the $\nu(C{=}N)_{oximate}$ modes of shi^{3-} would also be expected in this region. It is very likely that the strong bands at 1595/1432 and 1597/1432 cm^{-1} in the spectra of **1** and **2** are attributed to the

DOI: 10.1021/acs.inorgchem.7b01740
Inorg. Chem. 2017, 56, 10760−10774

$\nu_{as}(CO_2)$ and $\nu_s(CO_2)$ modes, respectively; the former should also involve a ring stretching character. The difference Δ [$\Delta = \nu_{as}(CO_2) - \nu_s(CO_2)$] is small (<165 cm^{-1}) in both cases, as is expected for the predominant bidentate bridging mode of carboxylate ligation (vide infra).[26,46] The bands at ~3060, ~2990, and ~2970 cm^{-1} in complexes **1**, **3**, and **4** can be assigned to the stretching vibrations of ν(N−H) modes from the presence of $NHEt_3^+$ countercations.[26,47] Finally, the carbonate-related IR bands in **4** could be tentatively assigned to the bands located at ~1448 and 863 cm^{-1}, as was previously observed in other carbonate-bridged metal complexes.[48]

Description of the Structures. The Mn oxidation states in all complexes **1**−**4** were established by charge-balance considerations, metric parameters, and bond-valence-sum (BVS;[49] Table 2) calculations. Selected interatomic distances and angles for complexes **1**−**4** are listed in Tables S1−S4, respectively. The crystal structure of **1** consists of $[Mn_4Ca_2(O_2CPh)_4(shi)_4(H_2O)_3(Me_2CO)]$ molecules (Figure 1, top) and lattice Me_2CO and H_2O solvate molecules; the latter two will not be further discussed.

Table 2. BVS Calculations[a] for Mn Atoms in Complexes 1−4

complex	atom	Mn^{II}	Mn^{III}	Mn^{IV}
1	Mn1	3.30	<u>3.05</u>	3.14
	Mn2	3.21	<u>2.97</u>	3.06
2	Mn1	<u>2.01</u>	1.65	1.68
	Mn2	3.21	<u>2.98</u>	3.06
	Mn3	3.20	<u>2.97</u>	3.05
3	Mn1	3.36	<u>3.11</u>	3.21
	Mn2	3.37	<u>3.12</u>	3.22
	Mn3	4.44	4.14	<u>4.22</u>
	Mn4	4.30	3.98	<u>4.10</u>
	Mn5	4.41	4.11	<u>4.19</u>
	Mn6	3.13	<u>2.90</u>	2.98
	Mn7	3.33	<u>3.09</u>	3.18
	Mn8	4.39	4.06	<u>4.19</u>
4	Mn1	3.37	<u>3.12</u>	3.21
	Mn2	3.36	<u>3.11</u>	3.20
	Mn3	3.34	<u>3.09</u>	3.18
	Mn4	3.36	<u>3.11</u>	3.20

[a]The underlined value is the one closest to the charge for which it was calculated. The oxidation state is the nearest whole number to the underlined value.

The centrosymmetric core of **1** comprises four Mn^{III} and two Ca^{II} atoms arranged in a slightly distorted octahedral topology (Figure 1, bottom right), with the Ca^{II} atoms occupying the apical positions and the Mn^{III} atoms forming the square base. The Mn···Mn···Mn angles are 89.7 and 90.3°, deviating only slightly from the ideal 90°, and the Mn···Ca···Mn angles of the eight triangular faces lie within the 75.6−77.5° range. The Mn^{III} atoms form a near-planar square, with each of the edges bridged by a diatomic oximate group from a shi^{3-} ligand, thus giving Mn···Mn separations of 4.623(1) and 4.652(1) Å. The almost perfectly planar Mn_4 unit is clearly due to the large Mn−O−N−Mn torsion angles of 176.7 and 177.6° for the Mn1−O2−N1−Mn2 and Mn2−O12′−N11′−Mn1′ units (and their symmetry-related counterparts), respectively, very close to the ideal linearity of 180°. The Ca^{II} atoms are displaced by 1.784 Å out of the Mn_4 best mean plane. The linkage between the basal Mn^{III} atoms and the apical Ca^{II} atoms is provided by the oximate O atoms (O2, O2′, O12, and O12′) of shi^{3-} ligands and the four $\eta^1:\eta^1:\mu$-bidentate-bridging benzoate groups; the latter are in pairs of two above and below the Mn_4 basal plane.

Ligation around each Mn^{III} atom is completed by the alkoxido and phenoxido O atoms from the shi^{3-} groups; the latter are thus $\eta^1:\eta^1:\eta^1:\eta^3:\mu_4$ (Scheme 3). The complex therefore contains an overall $[Mn_4Ca_2(\mu_3\text{-}NO)_4]^{12+}$ core (Figure 1, bottom left), which can also be described as a [12-$MC_{Mn^{III}N(shi)}$-4] metallacrown[50] with two Ca^{II} atoms displaced out of the arrangement. All Ca−O bonds are in the range 2.264(3)−2.595(3) Å. All Mn^{III} atoms in **1** are five-coordinate with almost perfect square-pyramidal geometries. This was confirmed by analysis of the shape-determining bond angles using the approach of Reedijk and co-workers,[51] which yields an average value for the trigonality index, τ, of 0.05 for the four metal ions, where τ is 0 and 1 for perfect square-pyramidal and trigonal-bipyramidal geometries, respectively. The Ca^{II} atoms are eight-coordinate in a CaO_8 environment possessing square-antiprismatic geometries. That was confirmed by the continuous-shape-measure (CShM) approach, which essentially allows one to numerically evaluate by how much a particular geometry deviates from an ideal shape.[52] The best fit was obtained for the square antiprism (Figure S1) with a CShM value of 2.21. Values of CShM between 0.1 and 3 usually correspond to a nonnegligible but still small distortion from ideal geometry.[53]

The coordination spheres of the Ca^{II} atoms in **1** are completed by three and one terminally bound H_2O and acetone molecules, respectively. Recall that four coordinated H_2O molecules were found in the active site of the native OEC, two of which are bound to the Ca^{II} atom. These H_2O molecules could serve as substrates for the overall catalytic reaction to proceed, including subsequent deprotonations with metal-centered oxidations preceding O−O bond formation.[54] To that end, complex **1** may be of some interest to the catalytic cycle of the OEC.

The crystal structure of **2** consists of $[Mn_6Ca_2Cl_2(O_2CPh)_7(shi)_4(py)_4]^-$ anions (Figure 2, top) counterbalanced by pyH^+ cations. In addition, there are CH_2Cl_2 and Et_2O solvate molecules in the crystal lattice, which will not be further discussed. The structure of the anion of **2** comprises a $\{Mn^{III}_4Ca_2\}$ octahedron, reminiscent of the discrete structure of complex **1**, linked to an additional $\{Mn^{II}_2\}$ dimer through two bridging Cl^- ions and two $\eta^2:\eta^2:\mu_4$ $PhCO_2^-$ groups (Scheme 3). The Mn···Mn···Mn angles within the $\{Mn^{III}_4Ca_2\}$ octahedron are 89.6 and 90.4°, again deviating only slightly from the ideal 90°, and the Mn···Ca···Mn angles of the eight triangular faces lie within the 74.5−79.0° range. The two Ca^{II} atoms lie 1.990 Å (Ca1) and 1.582 Å (Ca2) out of the Mn_4 square plane. Similar to complex **1**, the linkage between the basal Mn^{III} atoms and the apical Ca^{II} atoms is provided by the oximate O atoms (O1, O1′, O4, and O4′) of shi^{3-} ligands and four $\eta^1:\eta^1:\mu$-bidentate-bridging benzoate groups, which are all pointed toward Ca1. The two Mn^{II} atoms, which are located below Ca2, are further bridged to each other through an $\eta^1:\eta^1:\mu$ $PhCO_2^-$ group, while their coordination spheres are completed by four terminally bound pyridine molecules. The Mn^{II}···Mn^{II} distance is 3.400(1) Å. The overall metal topology of **2** (Figure 2, bottom right) and its $[Mn^{II}_2Mn^{III}_4Ca_2(\mu_3\text{-}Cl)_2(\mu_4\text{-}O_2CPh)_2(\mu_4\text{-}NO)_4]^{12+}$ core (Figure 2, bottom left) are finally stabilized by the coordinated alkoxido and phenoxido O atoms from the $\eta^1:\eta^1:\eta^1:\eta^3:\mu_4$ shi^{3-} groups.

DOI: 10.1021/acs.inorgchem.7b01740
Inorg. Chem. 2017, 56, 10760−10774

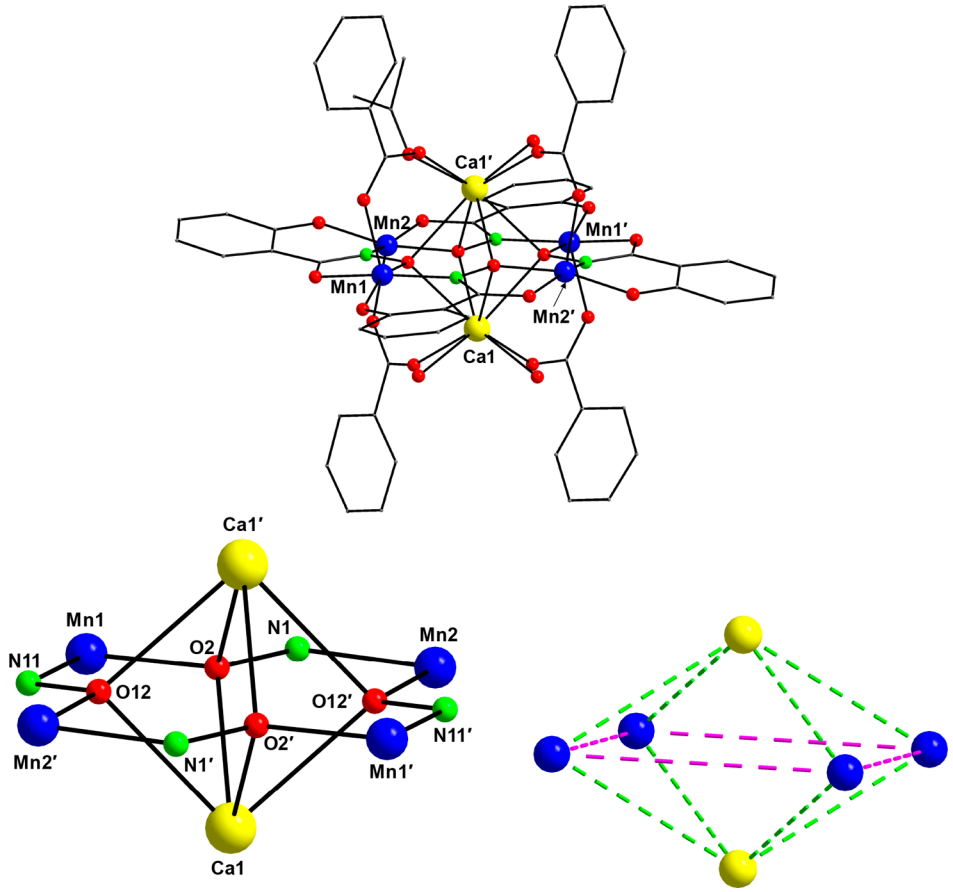

Figure 1. Partially labeled representations of the structure of **1** (top), its complete $[Mn_4Ca_2(\mu_3\text{-}NO)_4]^{12+}$ core (bottom, left), and the $\{Mn_4Ca_2\}$ octahedral topology (bottom, right). The green and purple dashed lines represent virtual Mn···Ca and Mn···Mn bonds. Color scheme: Mn^{III}, blue; Ca^{II}, yellow; O, red; N, green; C, gray. H atoms are omitted for clarity. Symmetry operation for the primed atoms in **1**: 0.5 − *x*, 0.5 − *y*, −*z*.

Scheme 3. Coordination Modes of All Bridging Ligands in Complexes 1−4

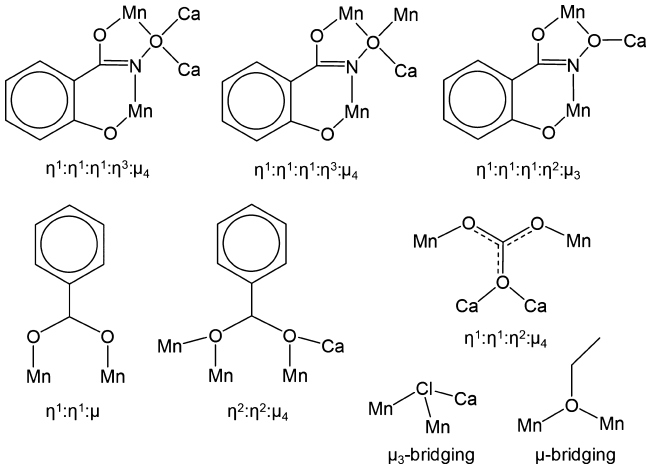

All Mn atoms in **2** are six-coordinate with distorted octahedral geometries. In the case of the Mn^{III} atoms (Mn2, Mn2′, Mn3, and Mn3′), the octahedra take the form of axially elongated Jahn−Teller (JT) distortions, as expected for high-spin d^4 ions in this geometry. The JT axes in all Mn^{III} sites involve the carboxylate O atoms and the Cl^- groups. In addition, both Ca^{II} atoms in **2** are eight-coordinate albeit with different coordination geometries, as established by CShM. The best fit was obtained for the square antiprism (Ca1) and biaugmented trigonal prism (Ca2) with CShM values of 1.19 and 3.98, respectively (Figure S2). Given the presence of Cl^- groups in the vicinity of the active site of the native OEC and their structural role in both maintaining the coordination environment of the $\{Mn_4Ca\}$ cluster and functioning as either proton exit channels or water inlet channels,[13] complex **2** could be structurally interesting because it is only, to the best of our knowledge, the second Cl-bridged Mn−Ca cluster reported to date (Table 3).

The crystal structure of **3** consists of $[Mn_8Ca(OEt)_2(shi)_{10}(EtOH)_2]^{2-}$ dianions (Figure 3, top), each of which is counterbalanced by two $NHEt_3^+$ cations. In addition, there are EtOH and H_2O solvate molecules in the crystal lattice, which will not be further discussed. The asymmetric dianion of **3** comprises four Mn^{III} (Mn1, Mn2, Mn6, and Mn7) and four Mn^{IV} (Mn3, Mn4, Mn5, and Mn8) atoms (Table 2), bridged together through the oximate groups of eight $\eta^1{:}\eta^1{:}\eta^1{:}\eta^2{:}\mu_3$ and two $\eta^1{:}\eta^1{:}\eta^1{:}\eta^3{:}\mu_4$ shi^{3-} groups (Scheme 3). Furthermore, there are also two EtO^- groups bridging two different pairs of Mn^{III} atoms (Mn1/Mn6 and Mn2/Mn7). The eight Mn atoms are arranged in a very distorted ringlike topology, with the four Mn^{III} and Mn^{IV} atoms being on opposite sides and the oximate O atoms serving to link the Mn_8 "ring" with the central Ca^{II} atom. As a result, the Ca^{II} atom is surrounded by 10 O atoms and possesses a coordination geometry that can be described as sphenocorona (CShM = 2.84; Figure S3). All Mn atoms are six-coordinate with near-octahedral geometries, while the axially elongated Mn^{III}

DOI: 10.1021/acs.inorgchem.7b01740
Inorg. Chem. 2017, 56, 10760−10774

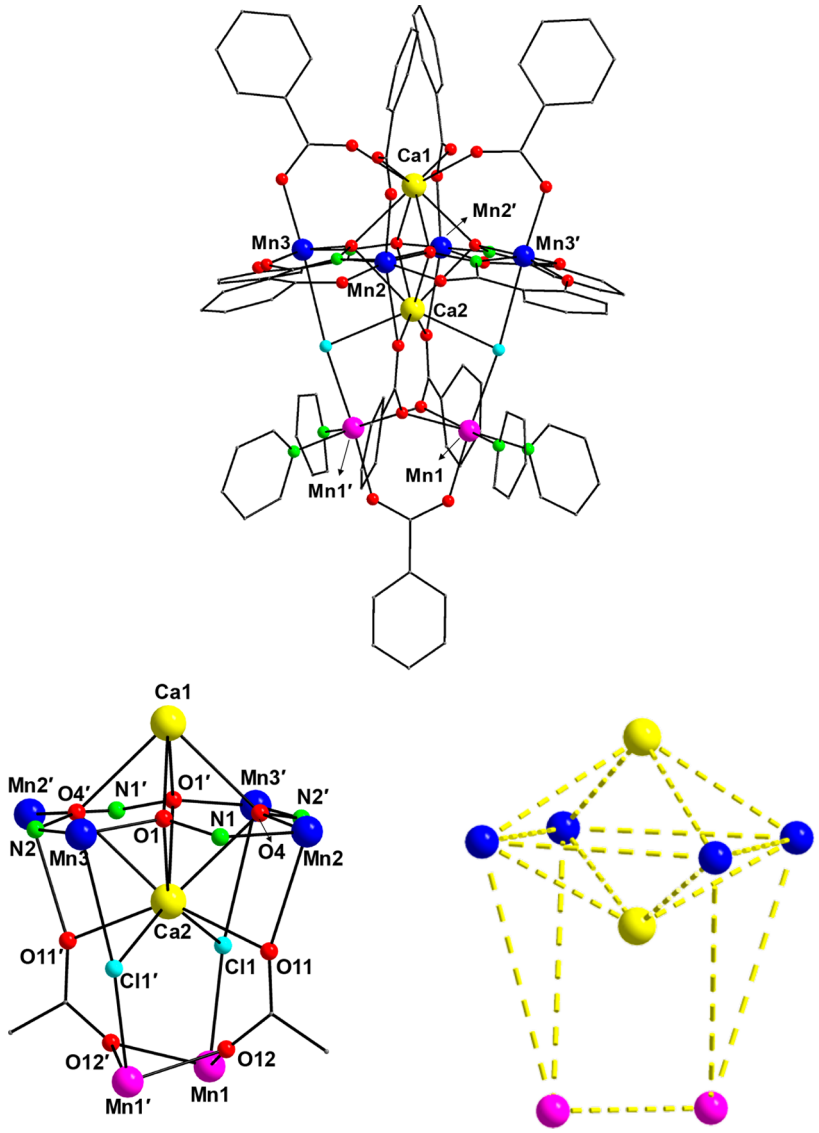

Figure 2. Partially labeled representations of the anion of complex **2** (top), its complete $[Mn^{II}_2Mn^{III}_4Ca_2(\mu_3\text{-}Cl)_2(\mu_4\text{-}O_2CPh)_2(\mu_3\text{-}NO)_4]^{12+}$ core (bottom, left), and the $\{Mn_6Ca_2\}$ topology (bottom, right). The yellow dashed lines represent virtual Mn···Ca and Mn···Mn bonds. Color scheme: Mn^{II}, purple; Mn^{III}, blue; Ca^{II}, yellow; O, red; N, green; Cl, cyan; C, gray. H atoms are omitted for clarity. Symmetry operation for the primed atoms in **2**: x, $0.5 - y$, $1.5 - z$.

octahedra are JT-distorted, with oximate and alkoxido O atoms occupying the four JT axes.

Complex **3** has an overall $[Mn^{III}_4Mn^{IV}_4Ca(\mu\text{-}OEt)_2(\mu_4\text{-}NO)_2(\mu_3\text{-}NO)_8]^{18+}$ core (Figure 3, bottom). The Mn···Mn and Mn···Ca distances span the ranges 3.283(1)−7.599(1) and 3.545(1)−4.048(1) Å, respectively, whereas the Mn−O−N−Mn torsion angles lie within the 96.9−174.7° range. The smallest torsion angles (~97−99°) are within the Mn^{III}···Mn^{III} pairs, and they deviate significantly from linearity. This is most likely the main reason for stabilization of the asymmetric structure of **3**, and consequently for the first time in Mn−Ca/shi^{3-} chemistry, we observed a structural motif that does not contain any discrete or repeating $\{Mn_4Ca\}$ square-pyramidal units. Finally, complex **3** is a rare example of a heterometallic Mn−Ca cluster containing both Mn^{III} and Mn^{IV} atoms, and the first non-oxido-bridged complex with an unprecedented 8:1 Mn-to-Ca metal ratio (Table 3).

The crystal structure of **4** consists of $[Mn_8Ca_2(CO_3)_4(shi)_8]^{4-}$ tetraanions (Figure 4, top), each of which is counterbalanced by four $NHEt_3^+$ cations. The latter cations are hydrogen-bonded with the coordinated carbonato O atoms. In addition, there are $CHCl_3$ solvate molecules in the crystal lattice, which will not be further discussed. The centrosymmetric complex $[Mn_8Ca_2(CO_3)_4(shi)_8]^{4-}$ is arranged as two parallel $\{Mn_4Ca\}$ square pyramids that are linked to each other through four $\eta^1{:}\eta^1{:}\eta^2{:}\mu_4$ CO_3^{2-} groups (Scheme 3). The two Ca^{II} atoms are both pointed toward the center of a cavity that is formed by the rectangular cuboidal (or rectangular parallelepiped) arrangement of the eight external Mn^{III} atoms (Figure 4, bottom right). As a result, the $\{Mn_8Ca_2\}$ compound possesses a virtual D_{2h} point group. The opposite faces of the rectangular cuboid comprise the atoms Mn(1,2,3,4)/Mn(1′,2′,3′,4′) and Mn(1,3,2′,4′)/Mn(1′,3′,2,4), with Mn···Mn distances spanning the ranges 4.612(3)−4.638(1) and 4.623(2)−6.122(3) Å, respectively. The Mn···Mn···Mn angles lie within the 89.7−90.1° range, very close to the ideal 90° for a perfect rectangular cuboid. The linkage between the basal Mn^{III} atoms and the apical Ca^{II} atoms within each $\{Mn_4Ca\}$ square

DOI: 10.1021/acs.inorgchem.7b01740
Inorg. Chem. 2017, 56, 10760−10774

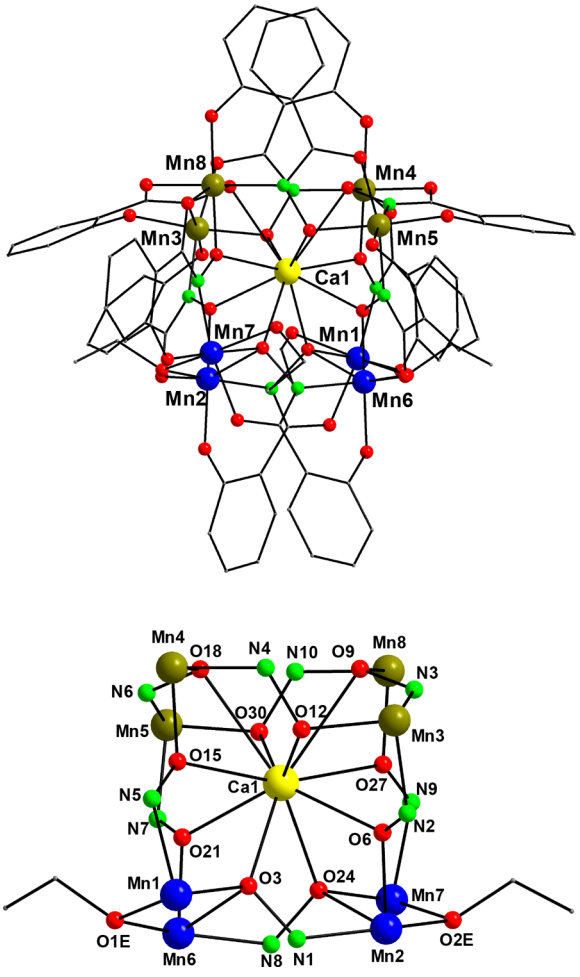

Figure 3. Partially labeled representations of the dianion of complex **3** (top) and its complete $[Mn^{III}_4Mn^{IV}_4Ca(\mu\text{-OEt})_2(\mu_4\text{-NO})_2(\mu_3\text{-NO})_8]^{18+}$ core (bottom). Color scheme: Mn^{III}, blue; Mn^{IV}, olive green; Ca^{II}, yellow; O, red; N, green; C, gray. H atoms are omitted for clarity.

pyramid is provided by the oximate O atoms (O1, O7, O6, and O18 and their symmetry-related partners) of eight shi^{3-} ligands; the latter are thus $\eta^1{:}\eta^1{:}\eta^1{:}\eta^2{:}\mu_3$ (Scheme 3). The four basal Mn^{III} atoms form a near-planar square, with each of the edges bridged by a diatomic oximate group from a shi^{3-} ligand. The almost perfectly planar Mn_4 units are clearly due to the large Mn−O−N−Mn torsion angles of ∼179°, very close to the ideal linearity of 180°. The linkage between the Mn atoms of the two $\{Mn_4Ca\}$ square pyramids is provided by the anti−anti O atoms of the four bridging CO_3^{2-} groups (Scheme 3). Ca1 and Ca1′ lie 1.556 Å below and above the corresponding Mn_4 best mean planes, respectively.

The complex therefore contains an overall $[Mn_8Ca_2(\mu_4\text{-}CO_3)_4(\mu_3\text{-NO})_8]^{12+}$ core (Figure 4, bottom left), which can also be described as two carbonato-bridged $[12\text{-}MC_{Mn^{III}N(shi)}\text{-}4]$ metallacrown units surrounding two Ca^{II} atoms. Alternatively, complex **4** can also be seen as a $\{Mn_8\}$ molecular "capsule" that accommodates two Ca^{II} atoms in its cavity (Figure 5). To the current degree of knowledge, a more possible scenario is that two solution-stable $\{Mn_4Ca\}$ units were assembled and linked together through the CO_3^{2-} groups rather than the two Ca^{II} atoms templating the formation of the outer $\{Mn_8\}$ unit. All Mn^{III} atoms in **4** are five-coordinate with almost perfect square-pyramidal geometries (τ = 0.07−0.09). Both Ca^{II} atoms are eight-coordinate in CaO_8 environments possessing square-antiprismatic geometries with a CShM value of 1.86 (Figure S4). Finally, complex **4** is the first heterometallic Mn−Ca complex bearing coordinated carbonato groups and the first Mn−Ca complex with an 8:2 metal stoichiometry (Table 3).

Considering the fast-developing field of heterometallic Mn−Ca chemistry, we felt timely to report in Table 3 all of the structurally characterized Mn−Ca cluster compounds reported to date, together with some of the most significant features from a bioinorganic perspective (i.e., metal stoichiometry, Mn oxidation states, and overall magnetic response). It becomes apparent that complexes **1**−**4** are quite unique in their metal-ion stoichiometries, topological arrangements, oxidation state descriptions, and the nature of the ligands bound to the metal ions.

Solid-State Magnetic Susceptibility Studies. Variable-temperature direct-current (dc) magnetic susceptibility measurements were performed on powdered polycrystalline samples of analytically pure complexes **1**·$2H_2O$, **2**, **3**·$2H_2O$, and **4**·$2CHCl_3$, restrained in eicosane to prevent torquing, in a 1 kG (0.1 T) field and in the 5.0−300 K range. The data are shown as $\chi_M T$ versus T plots in Figure 6. All complexes show very similar magnetic responses in terms of exhibiting a continuous decrease of their $\chi_M T$ products from 300 to 5 K. This is clearly due to the antiferromagnetic exchange interactions between the paramagnetic metal centers, undoubtedly propagated by the oximate bridges with very large (close to linearity) Mn−O−N−Mn torsion angles. This behavior is consistent with all previously characterized manganese/oximate complexes with large torsion angles.[26,69] More specifically, the $\chi_M T$ product for all four complexes steadily decreases from 9.28 (**1**), 17.53 (**2**), 15.03 (**3**), and 20.16 (**4**) cm^3 K mol^{-1} at 300 K to 0.74 (**1**), 0.87 (**2**), 0.88 (**3**), and 0.91 (**4**) cm^3 K mol^{-1} at 5.0 K. The 300 K values are less than the spin-only (g = 2) values of 12.00 (**1**), 20.75 (**2**), 19.50 (**3**), and 24.00 (**4**) cm^3 K mol^{-1} for the corresponding number of noninteracting Mn^{III} (**1** and **4**), $Mn^{II/III}$ (**2**), and $Mn^{III/IV}$ (**3**) ions. Given the very small $\chi_M T$ values for all complexes at low temperatures and the topological arrangement of the Mn atoms, it is very likely that compounds **1**−**4** all possess S = 0 spin ground-state values. This was confirmed quantitively by determining the individual pairwise exchange parameters J_{ij} between Mn_iMn_j pairs within the magnetic cores, when the overall topology and symmetry of the compound allowed us to do so.

To this end, the $\chi_M T$ versus T data for complex **1** were fit to the theoretical expression for a $\{Mn^{III}_4\}$ square using the isotropic Heisenberg spin Hamiltonian given by eq 5.

$$H = -2J(\hat{S}_1\cdot\hat{S}_2 + \hat{S}_2\cdot\hat{S}_3 + \hat{S}_3\cdot\hat{S}_4 + \hat{S}_1\cdot\hat{S}_4) \quad (5)$$

Considering the very similar Mn−O−N−Mn torsion angles and Mn···Mn separations within the Mn_4 square, all interactions between neighboring Mn^{III} atoms were considered as equivalent (1 − J model). The fit parameters were thus J and g. A good fit of the experimental data (red solid line in Figure 6) in the temperature range 300−15 K was obtained using the program *PHI* ($H = -2J_{ij}\hat{S}_i\cdot\hat{S}_j$ convention).[70] The best-fit parameters were J = −2.94(1) cm^{-1} and g = 1.96(1), in very good agreement with the previously reported $\{Mn^{III}_4Ca\}$ complexes possessing square-pyramidal topologies. Data below 15 K were omitted to avoid effects from Zeeman interactions, magnetic anisotropy, and crystal structure disorders; these are all factors that are not included in the above model.[26] The fit of the data indicates an S = 0 ground

DOI: 10.1021/acs.inorgchem.7b01740
Inorg. Chem. 2017, 56, 10760−10774

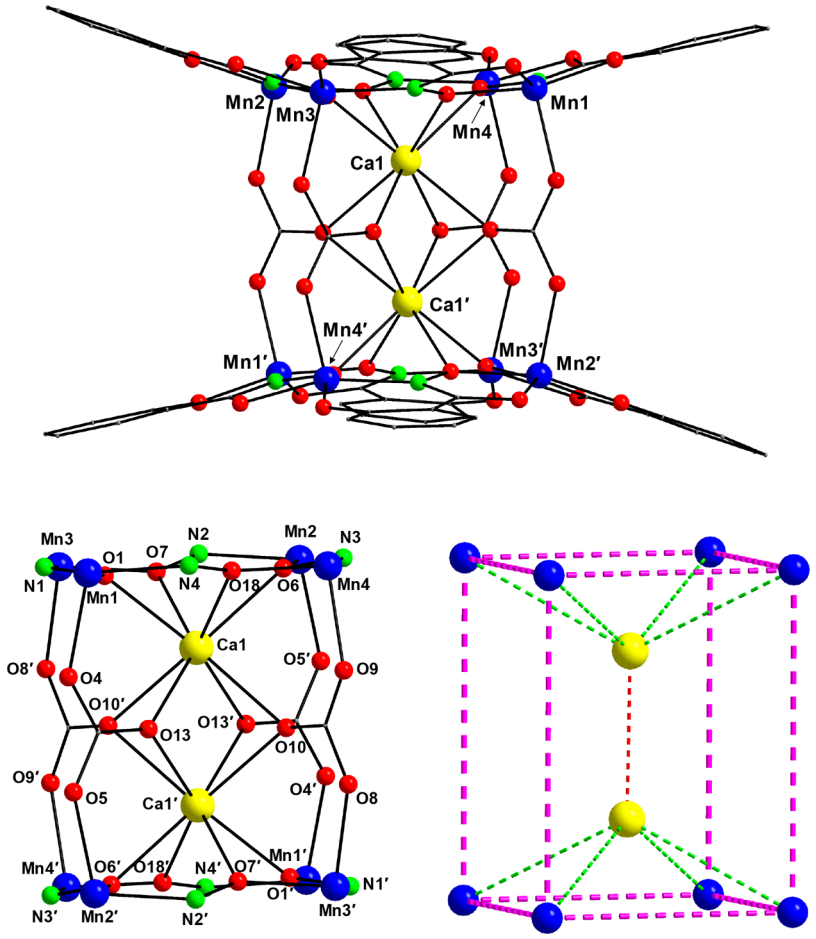

Figure 4. Partially labeled representations of the tetraanion of complex **4** (top), its complete $[Mn_8Ca_2(\mu_4\text{-}CO_3)_4(\mu_3\text{-}NO)_8]^{12+}$ core (bottom, left), and the $\{Mn_8Ca_2\}$ rectangular cuboidal topology (bottom, right). The green, purple, and red dashed lines represent virtual Mn···Ca, Mn···Mn, and Ca···Ca bonds. Color scheme: Mn^{III}, blue; Ca^{II}, yellow; O, red; N, green; C, gray. H atoms are omitted for clarity. Symmetry operation for the primed atoms in **4**: $-x, -y, -z$.

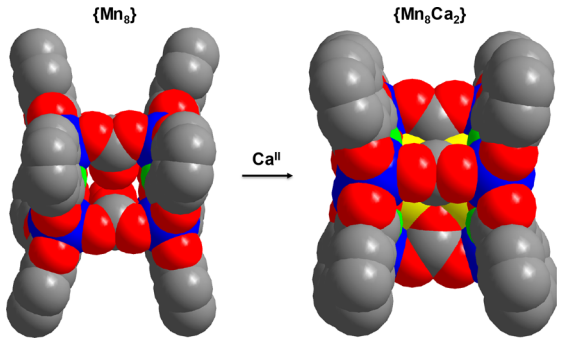

Figure 5. Space-filling representations of the "vacant" $\{Mn_8\}$ molecular "capsule" of **4** (left) and its complete $\{Mn_8Ca_2\}$ structure (right) resulting from the filling of the cavity by two Ca^{II} atoms. The color scheme is as in Figure 4.

state, with an $S = 1$ first excited state lying 5.88 cm^{-1} higher in energy. Attempts to include a D term in the fitting process and/or a second J coupling constant, to account for any nonzero next-nearest-neighbor interactions across the diagonal Mn sites, failed to give us any better low-temperature fits.

For the $\{Mn^{II}_2Mn^{III}_4Ca_2\}$ complex **2**, we employed a similar Heisenberg spin Hamiltonian (eq 6), but this time two coupling constants were included to account for the interactions between the Mn^{III} atoms within the $\{Mn_4\}$ square (J_1), as promoted by the oximate bridges, and the interaction between the two carboxylate-bridged Mn^{II} atoms (J_2). The best-fit parameters were $J_1 = -2.88(1)$ cm^{-1}, $J_2 = -4.13(1)$ cm^{-1}, and $g = 1.95(1)$, and these were derived from the program *PHI* for the entire temperature range (blue solid line in Figure 6), thus confirming the overall antiferromagnetic response of the compound and stabilization of an $S = 0$ spin ground state.

$$H = -2J_1(\hat{S}_2\cdot\hat{S}_3 + \hat{S}_3\cdot\hat{S}_{2'} + \hat{S}_{2'}\cdot\hat{S}_{3'} + \hat{S}_{3'}\cdot\hat{S}_2) - 2J_2(\hat{S}_1\cdot\hat{S}_{1'}) \quad (6)$$

The employment of a third J coupling constant to consider any possible interaction between the Mn^{II} and Mn^{III} atoms gave us a negligible value (~0 cm^{-1}). This is reasonable because the Mn^{II} and Mn^{III} atoms in **2** are solely bridged by the Cl^- groups, which are expected to provide a very weak to negligible superexchange magnetic pathway when forming an almost linear angle between the metal centers [Mn1−Cl1−Mn3′ = 169.8(1)°], and the bonding is weak as well [Mn1−Cl1 = 2.486(1) Å and Mn3−Cl1 = 2.870(3) Å].

The larger nuclearities and low symmetries of complexes **3** and **4** rendered the fitting of the magnetic data impossible. A powerful complement to dc studies for determining the ground state of a system is alternating-current (ac) magnetic susceptibility measurements, which preclude any complications

DOI: 10.1021/acs.inorgchem.7b01740
Inorg. Chem. 2017, 56, 10760−10774

Table 3. Chemical Formulas, Structural Details, and Ground-State S Values for the Mn−Ca Cluster Compounds Reported to Date

formula[a]	metal stoichiometry	Mn oxidation state	S[b]	ref
$[Mn_3CaO_3(OH)(L1)(ON_4O)(O_2CMe)]^+$	3Mn/1Ca	$3Mn^{IV}$	n.r.	55
$[Mn_3CaO_4(L1)(ON_4O)(O_2CMe)]$	3Mn/1Ca	$3Mn^{IV}$	n.r.	55
$[Mn_3CaAgO_4(L1)(ON_4O)(O_2CMe)(OTf)]$	3Mn/1Ca	$3Mn^{IV}$	n.r.	55
$[Mn_3CaO_4(L1)(O_2CMe)_3(THF)]$	3Mn/1Ca	$3Mn^{IV}$	n.r.	22
$[Mn_6CaO_2(L1)_2(O_2CMe)_6]^{2+}$	6Mn/1Ca	$2Mn^{II},4Mn^{III}$	n.r.	22
$[Mn_3CaO_2(L1)(O_2CMe)_2(DME)(OTf)]^{2+}$	3Mn/1Ca	$2Mn^{III},1Mn^{IV}$	$^{11}/_2$	56
$[Mn_3CaO_2(L1)(O_2CMe)_2(DME)(OTf)]^+$	3Mn/1Ca	$3Mn^{III}$	n.r.	56
$[Mn_3CaO_2(L1)(O_2CMe)_2(H_2O)_3]^{3+}$	3Mn/1Ca	$2Mn^{III},1Mn^{IV}$	n.r.	56
$[Mn_3CaNaO(L2)_3(N_3)_3(MeOH)]^+$	3Mn/1Ca	$3Mn^{III}$	n.r.	57
$[Mn_{13}Ca_2O_{10}(OH)_2(OMe)_2(O_2CPh)_{18}(H_2O)_4]$	13Mn/2Ca	$2Mn^{II},10Mn^{III},1Mn^{IV}$	$^5/_2$	58
$[Mn_4CaO_4(O_2CBu^t)_8(Bu^tCO_2H)_2(py)]$	4Mn/1Ca	$2Mn^{III},2Mn^{IV}$	n.r.	23
$[Mn_4CaO_4(O_2CBu^t)_8(Bu^tCO_2H)(py)_2]$	4Mn/1Ca	$2Mn^{III},2Mn^{IV}$	n.r.	23
$[Mn_4CaO_4(O_2CBu^t)_8(Bu^tCO_2H)_2(qn)]$	4Mn/1Ca	$2Mn^{III},2Mn^{IV}$	n.r.	23
$[Mn_6Ca_2O_2(Me\text{-}sao)_6(O_2CEt)_6(H_2O)_2]_n$	6Mn/2Ca	$6Mn^{III}$	4	59
$[Mn_4CaOCl_3(L3)_3(O_2CMe)(H_2O)_{1.5}(MeOH)_{0.3}]^+$	4Mn/1Ca	$1Mn^{II},3Mn^{III}$	$^1/_2$	60
$[Mn_2Ca_2(L4)_2(DMF)_4]$	2Mn/2Ca	$2Mn^{II}$	n.r.	61
$[MnCa_2(L4H)_2(DMF)_4]$	1Mn/2Ca	$1Mn^{II}$	n.r.	61
$[Mn_3CaNa(sal)_6(H_2O)_6]_n$	3Mn/1Ca	$3Mn^{III}$	n.r.	62
$[Mn_2Ca_2(tpaa)_2(H_2O)_{12}][Mn(tpaa)]_2$	2Mn/2Ca	$2Mn^{II}$	n.r.	63
$[MnCa_2(Hcit)_2(H_2O)_4]_n$	1Mn/2Ca	$1Mn^{II}$	n.r.	64
$[Mn_6Ca_2O_9(O_2CBu^t)_{10}(H_2O)_4]$	6Mn/2Ca	$6Mn^{IV}$	n.r.	65
$[Mn_6Ca_2O_9(O_2CBu^t)_{10}(H_2O)_3(CH_3CO_2C_2H_5)]$	6Mn/2Ca	$6Mn^{IV}$	n.r.	65
$[Mn_6Ca_2O_9(O_2CBu^t)_{11}][Mn_3O(O_2CBu^t)_6(py)_3]$	6Mn/2Ca	$6Mn^{IV}$	n.r.	65
$[Mn_4Ca_2Cl_4(OEtOMe)_8]$	4Mn/2Ca	$4Mn^{II}$	n.r.	66
$[MnCa_2(O_2CCCl_2)_6(bipy)_2(H_2O)(MeOH)]$	1Mn/2Ca	$1Mn^{II}$	$^5/_2$	67
$[Mn_3Ca_2O_4(O_2CBu^t)_8(Bu^tCO_2H)_4]$	3Mn/2Ca	$3Mn^{IV}$	$^9/_2$	24
$[Mn_6Ca_2O_9(O_2CPhBu^t)_{10}(Bu^tPhCO_2H)_5]$	6Mn/2Ca	$6Mn^{IV}$	0	68
$[Mn_4Ca(O_2CPh)_4(shi)_4]^{2-}$	4Mn/1Ca	$4Mn^{III}$	0	26
$[Mn_4Ca(L5)_4(shi)_4]^{2-}$	4Mn/1Ca	$4Mn^{III}$	0	26
$[Mn_4Ca(L6)_4(shi)_4]^{2-}$	4Mn/1Ca	$4Mn^{III}$	0	26
$[Mn_4Ca(L6)_4(shi)_4(shiH_2)_2]^{4-}$	4Mn/1Ca	$4Mn^{III}$	0	26
$[Mn_4Ca(L7)_4(shi)_4]^{2-}$	4Mn/1Ca	$4Mn^{III}$	0	26
$[Mn_4Ca_2(O_2CPh)_4(shi)_4(H_2O)_2(Me_2CO)_2]$ (**1**)	4Mn/2Ca	$4Mn^{III}$	0	t.w.
$[Mn_6Ca_2Cl_2(O_2CPh)_7(shi)_4(py)_4]^-$ (**2**)	6Mn/2Ca	$2Mn^{II},4Mn^{III}$	0	t.w.
$[Mn_8Ca(OEt)_2(shi)_{10}(EtOH)_2]^{2-}$ (**3**)	8Mn/1Ca	$4Mn^{III},4Mn^{IV}$	0	t.w.
$[Mn_8Ca_2(CO_3)(shi)_8]^{4-}$ (**4**)	8Mn/2Ca	$8Mn^{III}$	0	t.w.

[a]Excluding all lattice solvate molecules and counterions. Abbreviations: n.r. = not reported; t.w. = this work; $L1H_3$ = 1,3,5-tris[2-di-2′-pyridylhydroxymethylphenyl]benzene; THF = tetrahydrofuran; HON_4OH = *N*,*N*′-dimethyl-*N*,*N*′-diacetylethylenediamine dioxime; OTf^- = trifluoromethanesulfonate; $L2H_3$ = 2-(2,3-dihydroxypropyliminomethyl)-6-methoxyphenol; $L3H_2$ = 2-[[(2-hydroxypropyl)imino]methyl]-6-methoxyphenol; $L4H_4$ = *p*-*tert*-butylthiacalix[4]arene; DME = 1,2-dimethoxyethane; qn = isoquinoline; Me-saoH_2 = 2-hydroxyphenylethanone oxime; L5H = 2-naphthoic acid; L6H = 9-anthracenecarboxylic acid; L7H = 1-pyrenecarboxylic acid; DMF = dimethylformamide; H_2sal = salicylic acid; H_3tpaa = 6,6′,6″-nitrilotris(methylene)tripicolinic acid; H_4cit = citric acid; MeOEtOH = 2-methoxyethanol; bipy = 2,2′-bipyridine; Bu^tPhCO_2H = *p*-*tert*-butylbenzoic acid. [b]From magnetic susceptibility data.

arising from the presence of a dc field. These were performed for both **3** and **4** in a 3.5 G ac field oscillating at different frequencies. The in-phase susceptibility (χ_M') is shown as $\chi_M'T$ versus T plots in Figure S5 and reveals some pertinent and common features for both complexes **3** and **4**: (i) $\chi_M'T$ decreases linearly with decreasing temperature in the 1.8−14 K range, indicating depopulation of a high density of excited states with spin S greater than that of the ground state; (ii) linear extrapolation of the $\chi_M'T$ data down to 0 K gives a value of ∼0 cm^3 K mol^{-1} for both **3** and **4**, indicative of S = 0 ground states.

Relevance of Complexes 1−4 to Different Oxidation States of the OEC: A Qualitative Approach. A qualitative and brief discussion of the relevance of complexes **1**−**4** to some species of the native OEC is herein attempted. In addition to the bridging/chelating shi^{3-} ligand, most of the reported compounds contain carboxylate, chloride, water, and/or carbonate groups akin to the coordination environment of the metal ions in the native enzyme. We recognize that, within the structures of **1**−**4**, the Mn···Mn (between closest neighbors) and Mn···Ca separations span the ranges 4.623−4.652 and 3.680−3.773 Å (**1**), 4.624−6.283 and 3.620−3.856 Å (**2**), 3.180−6.639 and 3.545−4.048 Å (**3**), and 4.612−6.122 and 3.601−3.635 Å (**4**), respectively; these values are significantly larger than the corresponding values of 2.7−3.3 and ∼3.4 Å for the OEC in PSII. This is clearly due to the absence of bridging oxido groups and the presence of Mn^{II}/Mn^{III} atoms within **1**−**4**. However, the structures of the reported compounds may be of some relevance to the OEC in other ways. Because the S_1 Kok state of the OEC occurs at the

DOI: 10.1021/acs.inorgchem.7b01740
Inorg. Chem. 2017, 56, 10760−10774

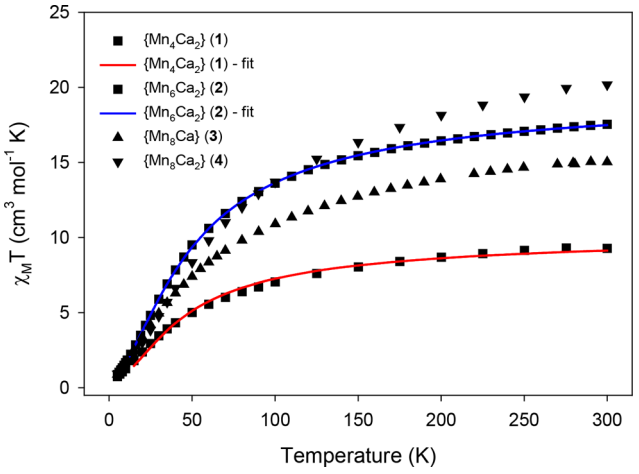

Figure 6. $\chi_M T$ versus T plots for complexes **1**−**4** at 0.1 T dc field. The red and blue solid lines are the fits of the corresponding data; see the text for the fit parameters.

$2Mn^{III}$,$2Mn^{IV}$ oxidation level with a ground-state spin of $S = 0$, then the $Mn^{III}_4Mn^{IV}_4$ level of **3** could be related to this S_1 state. In contrast, the lower Mn^{III}_4, $Mn^{II}_2Mn^{III}_4$, and Mn^{III}_8 levels of **1**, **2**, and **4**, respectively, would place them at the S_{-1} or other reduced states of the catalytic cycle. Hydrazine (N_2H_4), hydroxylamine (NH_2OH), and nitric oxide can reduce the OEC to S_{-1}, S_{-2}, and even S_{-3} states.[71] These are not involved in the water oxidation catalytic cycle but may be related to intermediates during the in vivo assembly of the OEC. Assuming these involve Mn-based reductions, then they would be at the $4Mn^{III}$,Mn^{II},$3Mn^{III}$ and $2Mn^{II}$,$2Mn^{III}$ levels, respectively; an EPR signal assignable to a $Mn^{II}Mn^{III}$ subunit has been detected for S_{-2}.[72] Furthermore, the similarity between the oximate N−O bridging unit of shi^{3-} within **1**−**4** and the M−N−O−M unit found in hydroxylamine-bridged metal complexes[73] is interesting and suggests that **1**−**4** may be providing insight into the types of subunits that might be generated upon reduction of the OEC with NH_2OH.

CONCLUSIONS

In conclusion, we have shown that $shiH_3$ is a versatile chelating/bridging ligand that can support the formation of heterometallic Mn−Ca clusters with unprecedented topologies, metal stoichiometries, and oxidation-state descriptions. The reaction schemes employed in this work were quite diverse, ranging from the use of $\{Mn^{III}_3\}$ and $\{Mn^{II/III}_3\}$ oxido/carboxylate-based triangles to simple Mn^{II} and Ca^{II} starting materials, and the resulting crystalline products were proven to exhibit different structural motifs and ancillary bridging ligands, such as $PhCO_2^-$, EtO^-, Cl^-, and CO_3^{2-}. The combined results also demonstrate the ability of shi^{3-} to stabilize Mn ions in high oxidation states (i.e., Mn^{IV}) without requiring the support of oxido groups. It must be admitted that the cores and metal stoichiometries of **1**−**4** are different from the extended $\{Mn_4Ca\}$ cubane core of the native OEC. This, however, does not preclude some relevance of the reported compounds to both the high-valent scheme ($Mn^{III}_4Mn^{IV}_4$; **3**) and lower-oxidation-level species (**1**, **2**, and **4**) that are intermediates during the assembly of the OEC in vivo or those generated by treatment of the OEC with strong reducing agents.

We are still seeking ways and new synthetic conditions to stabilize Mn−Ca/shi^{3-} complexes with coordinated and bridging O^{2-} groups, as a means of obtaining heterometallic cluster compounds with more relevance to the S_0−S_3 states within the high-valent scheme of the catalytic Kok cycle. In addition, work in progress includes the synthesis and systematic investigation of various new hydroxamic acids and oxime-based ligands in Mn−Ca coordination chemistry. Finally, the $\{Mn_4Ca_2\}$ octahedral arrangement of **1** is very similar to the one seen before in Mn−Ce chemistry albeit with different bridging and ancillary ligands.[74] This is important when targeting the deliberate replacement of Ca^{II} atoms by paramagnetic and anisotropic 4f metal ions in an attempt to synthesize molecule-based magnets.

ASSOCIATED CONTENT

Supporting Information

The Supporting Information is available free of charge on the ACS Publications website at DOI: 10.1021/acs.inorgchem.7b01740.

Selected interatomic distances and angles, coordination polyhedra for all Ca atoms, and $\chi_M'T$ versus T (PDF)

Accession Codes

CCDC 1559398−1559399, 1559579, and 1559957 contain the supplementary crystallographic data for this paper. These data can be obtained free of charge via www.ccdc.cam.ac.uk/data_request/cif, or by emailing data_request@ccdc.cam.ac.uk, or by contacting The Cambridge Crystallographic Data Centre, 12 Union Road, Cambridge CB2 1EZ, UK; fax: +44 1223 336033.

AUTHOR INFORMATION

Corresponding Author

*E-mail: tstamatatos@brocku.ca.

ORCID

Laura J. McCormick: 0000-0002-6634-4717

Theocharis C. Stamatatos: 0000-0002-9798-9331

Notes

The authors declare no competing financial interest.

ACKNOWLEDGMENTS

This work was supported by NSERC-DG, ERA, and Brock University (Chancellor's Chair for Research Excellence; all to Th.C.S) and NSF Grant CHE-1410394 (to G.C.). A.A.A. thanks Queen Elizabeth II Graduate Scholarships in Science and Technology for supporting this work. L.C.-S. acknowledges financial support from FCT/MCTES (Fundação para a Ciência e a Tecnologia/Ministério da Ciência, Tecnologia e Ensino Superior, Portugal) with national funds and was also cofinanced by FEDER (Fundo Europeu de Desenvolvimento Regional, European Union) under Partnership Agreement PT2020, through the research centre REQUIMTE-LAQV (UID/QUI/50006/2013-POCI/01/0145/FEDER/007265). A.E. acknowledges financial support from Ministerio de Economía y Competitividad (Project CTQ2015-63614-P). The Advanced Light Source is supported by the Director, Office of Science, Office of Basic Energy Sciences, U.S. Department of Energy, under Contract DE-AC02-05CH11231.

REFERENCES

(1) (a) Wydrzynski, T.; Satoh, K. *The Light-Driven Water: Plastoquinone Oxidoreductase*; Springer: Dordrecht, The Netherlands, 2005; Vol. 22. (b) McEvoy, J. P.; Brudvig, G. W. Water-Splitting

DOI: 10.1021/acs.inorgchem.7b01740
Inorg. Chem. 2017, 56, 10760−10774

Chemistry of Photosystem II. *Chem. Rev.* **2006**, *106*, 4455−4483. (c) Yano, J.; Yachandra, V. Mn_4Ca Cluster in Photosynthesis: Where and How Water is Oxidized to Dioxygen. *Chem. Rev.* **2014**, *114*, 4175−4205.

(2) For representative references, see: (a) Mukhopadhyay, S.; Mandal, S. K.; Bhaduri, S.; Armstrong, W. H. Manganese Clusters with Relevance to Photosystem II. *Chem. Rev.* **2004**, *104*, 3981−4026. (b) Pecoraro, V. L.; Hsieh, W.-Y. In Search of Elusive High-Valent Manganese Species That Evaluate Mechanisms of Photosynthetic Water Oxidation. *Inorg. Chem.* **2008**, *47*, 1765−1778. (c) Meelich, K.; Zaleski, C. M.; Pecoraro, V. L. Using small molecule complexes to elucidate features of photosynthetic water oxidation. *Philos. Trans. R. Soc., B* **2008**, *363*, 1271−1281.

(3) (a) Barber, J. Photosynthetic energy conversion: natural and artificial. *Chem. Soc. Rev.* **2009**, *38*, 185−196. (b) Nocera, D. G. The Artificial Leaf. *Acc. Chem. Res.* **2012**, *45*, 767−776. (c) Cox, N.; Pantazis, D. A.; Neese, F.; Lubitz, W. Artificial photosynthesis: understanding water splitting in nature. *Interface Focus* **2015**, *5*, 20150009.

(4) Yano, J.; Kern, J.; Sauer, K.; Latimer, M. J.; Pushkar, Y.; Biesiadka, J.; Loll, B.; Saenger, W.; Messinger, J.; Zouni, A.; Yachandra, V. K. Where Water Is Oxidized to Dioxygen: Structure of the Photosynthetic Mn_4Ca Cluster. *Science* **2006**, *314*, 821−825.

(5) (a) Barber, J. Mn_4Ca Cluster of Photosynthetic Oxygen-Evolving Center: Structure, Function and Evolution. *Biochemistry* **2016**, *55*, 5901−5906. (b) Shen, J.- R. The Structure of Photosystem II and the Mechanism of Water Oxidation in Photosynthesis. *Annu. Rev. Plant Biol.* **2015**, *66*, 23−48.

(6) (a) Zouni, A.; Witt, H.- T.; Kern, J.; Fromme, P.; Krauss, N.; Saenger, W.; Orth, P. Crystal Structure of Photosystem II from *Synechococcus Elongatus* at 3.8 Å Resolution. *Nature* **2001**, *409*, 739−743. (b) Peloquin, J. M.; Campbell, K. A.; Randall, D. W.; Evanchik, M. A.; Pecoraro, V. L.; Armstrong, W. H.; Britt, R. D. ^{55}Mn ENDOR of the S_2-State Multiline EPR Signal of Photosystem II: Implications on the Structure of the Tetranuclear Mn Cluster. *J. Am. Chem. Soc.* **2000**, *122*, 10926−10942. (c) Pantazis, D. A.; Ames, W.; Cox, N.; Lubitz, W.; Neese, F. Two Interconvertible Structures that Explain the Spectroscopic Properties of the Oxygen-Evolving Complex of Photosystem II in the S_2 State. *Angew. Chem., Int. Ed.* **2012**, *51*, 9935−9940.

(7) Brynda, M.; Britt, R. D. The Manganese−Calcium Cluster of the Oxygen-Evolving System: Synthetic Models, EPR Studies, and Electronic Structure Calculations. In *Metals in Biology: Applications of High-Resolution EPR to Metalloenzymes*; Hanson, G., Berliner, L., Eds.; Springer: New York, 2010; pp 203−271.

(8) (a) Kok, B.; Forbush, B.; McGloin, M. Cooperation of Charges in Photosynthetic O_2 Evolution-I. A Linear Four Step Mechanism. *Photochem. Photobiol.* **1970**, *11*, 457−475. (b) Joliot, P.; Barbieri, G.; Chabaud, R. Un Nouveau Modele Des Centees Photochimiques Du System II. *Photochem. Photobiol.* **1969**, *10*, 309−329.

(9) (a) Visser, H.; Anxolabéhère-Mallart, E.; Bergmann, U.; Glatzel, P.; Robblee, J. H.; Cramer, S. P.; Girerd, J.- J.; Sauer, K.; Klein, M. P.; Yachandra, V. K. Mn K-Edge XANES and Kβ XES Studies of Two Mn-Oxo Binuclear Complexes: Investigation of Three Different Oxidation States Relevant to the Oxygen-Evolving Complex of Photosystem II. *J. Am. Chem. Soc.* **2001**, *123*, 7031−7039. (b) Pecoraro, V. L.; Baldwin, M. J.; Caudle, M. T.; Hsieh, W.- Y.; Law, N. A. A proposal for water oxidation in photosystem II. *Pure Appl. Chem.* **1998**, *70*, 925−929.

(10) (a) Haumann, M.; Liebisch, P.; Müller, C.; Barra, M.; Grabolle, M.; Dau, H. Photosynthetic O_2 Formation Tracked by Time-Resolved X-ray Experiments. *Science* **2005**, *310*, 1019−1021. (b) Kolling, D. R. J.; Cox, N.; Ananyev, G. M.; Pace, R. J.; Dismukes, G. C. What Are the Oxidation States of Manganese Required to Catalyze Photosynthetic Water Oxidation? *Biophys. J.* **2012**, *103*, 313−322.

(11) Loll, B.; Kern, J.; Saenger, W.; Zouni, A.; Biesiadka, J. Towards complete cofactor arrangement in the 3.0 Å resolution structure of photosystem II. *Nature* **2005**, *438*, 1040−1044.

(12) Tsui, E. Y.; Kanady, J. S.; Agapie, T. Synthetic Cluster Models of Biological and Heterogeneous Manganese Catalysts for O_2 Evolution. *Inorg. Chem.* **2013**, *52*, 13833−13848.

(13) Umena, Y.; Kawakami, K.; Shen, J.- R.; Kamiya, N. Crystal structure of oxygen-evolving photosystem II at a resolution of 1.9 Å. *Nature* **2011**, *473*, 55−60.

(14) Krewald, V.; Retegan, M.; Cox, N.; Messinger, J.; Lubitz, W.; DeBeer, S.; Neese, F.; Pantazis, D. A. Metal oxidation states in biological water splitting. *Chem. Sci.* **2015**, *6*, 1676−1695.

(15) (a) Miller, A.- F.; Brudvig, G. W. Electron-Transfer Events Leading to Reconstitution of Oxygen-Evolution Activity in Manganese-Depleted Photosystem II Membranes. *Biochemistry* **1990**, *29*, 1385−1392. (b) Burnap, R. L. D1 protein processing and Mn cluster assembly in light of the emerging Photosystem II structure. *Phys. Chem. Chem. Phys.* **2004**, *6*, 4803−4809.

(16) (a) Campbell, K. A.; Force, D. A.; Nixon, P. J.; Dole, F.; Diner, B. A.; Britt, R. D. Dual-Mode EPR Detects the Initial Intermediate in Photoassembly of the Photosystem II Mn Cluster: The Influence of Amino Acid Residue 170 of the D1 Polypeptide on Mn Coordination. *J. Am. Chem. Soc.* **2000**, *122*, 3754−3761. (b) Dasgupta, J.; Ananyev, G. M.; Dismukes, G. C. Photoassembly of the water-oxidizing complex in photosystem II. *Coord. Chem. Rev.* **2008**, *252*, 347−360.

(17) Brudvig, G. W.; Beck, W. F. Biomimetic Oxidations Catalyzed by Transition Metal Complexes. In *Manganese Redox Enzymes*; Pecoraro, V. L., Ed.; VCH Publishers, Inc.: New York, 1992; pp 119−140.

(18) Schansker, G.; Goussias, C.; Petrouleas, V.; Rutherford, A. W. Reduction of the Mn Cluster of the Water-Oxidizing Enzyme by Nitric Oxide: Formation of an S_{-2} State. *Biochemistry* **2002**, *41*, 3057−3064.

(19) Kanady, J. S.; Tran, R.; Stull, J. A.; Lu, L.; Stich, T. A.; Day, M. W.; Yano, J.; Britt, R. D.; Agapie, T. Role of oxido incorporation and ligand lability in expanding redox accessibility of structurally related Mn_4 cluster. *Chem. Sci.* **2013**, *4*, 3986−3996.

(20) For recent reviews in polynuclear Mn clusters, see: (a) Kostakis, G. E.; Blatov, V. A.; Proserpio, D. M. A method for topological analysis of high nuclearity coordination clusters and its application to Mn coordination compounds. *Dalton Trans.* **2012**, *41*, 4634−4640. (b) Aromí, G.; Brechin, E. K. Synthesis of 3d Metallic Single-Molecule Magnets. *Struct. Bonding (Berlin)* **2006**, *122*, 1−67. (c) Papatriantafyllopoulou, C.; Moushi, E. E.; Christou, G.; Tasiopoulos, A. J. Filling the gap between the quantum and classical worlds of nanoscale magnetism: giant molecular aggregates based on paramagnetic 3d metal ions. *Chem. Soc. Rev.* **2016**, *45*, 1597−1628.

(21) Gerey, B.; Gouré, E.; Fortage, J.; Pécaut, J.; Collomb, M.- N. Manganese-calcium/strontium heterometallic compounds and their relevance for the oxygen-evolving center of photosystem II. *Coord. Chem. Rev.* **2016**, *319*, 1−24.

(22) Kanady, J. S.; Tsui, E. Y.; Day, M. W.; Agapie, T. A Synthetic Model of the Mn_3Ca Subsite of the Oxygen-Evolving Complex in Photosystem II. *Science* **2011**, *333*, 733−736.

(23) Zhang, C.; Chen, C.; Dong, H.; Shen, J.- R.; Dau, H.; Zhao, J. A synthetic Mn_4Ca-cluster mimicking the oxygen-evolving center of photosynthesis. *Science* **2015**, *348*, 690−693.

(24) Mukherjee, S.; Stull, J. A.; Yano, J.; Stamatatos, T. C.; Pringouri, K.; Stich, T. A.; Abboud, K. A.; Britt, R. D.; Yachandra, V. K.; Christou, G. Synthetic model of the asymmetric $[Mn_3CaO_4]$ cubane core of the oxygen-evolving complex of photosystem II. *Proc. Natl. Acad. Sci. U. S. A.* **2012**, *109*, 2257−2262.

(25) Paul, S.; Neese, F.; Pantazis, D. A. Structural models of the biological oxygen-evolving complex: achievements, insights, and challenges for biomimicry. *Green Chem.* **2017**, *19*, 2309−2325.

(26) (a) Koumousi, E. S.; Mukherjee, S.; Beavers, C. M.; Teat, S. J.; Christou, G.; Stamatatos, T. C. Towards models of the oxygen-evolving complex (OEC) of photosystem II: a Mn_4Ca cluster of relevance to low oxidation states of the OEC. *Chem. Commun.* **2011**, *47*, 11128−11130. (b) Alaimo, A. A.; Takahashi, D.; Cunha-Silva, L.; Christou, G.; Stamatatos, T. C. Emissive $\{Mn_4Ca\}$ Clusters with Square Pyramidal Topologies: Syntheses and Structural, Spectro-

DOI: 10.1021/acs.inorgchem.7b01740
Inorg. Chem. 2017, 56, 10760−10774

scopic, and Physicochemical Characterization. *Inorg. Chem.* **2015**, *54*, 2137−2151.
(27) For some representative references, see: (a) Zaleski, C. M.; Kampf, J. W.; Mallah, T.; Kirk, M. L.; Pecoraro, V. L. Assessing the Slow Magnetic Relaxation Behavior of $Ln^{III}_4Mn^{III}_6$ Metallacrowns. *Inorg. Chem.* **2007**, *46*, 1954−1956. (b) Boron, T. T., III; Kampf, J. W.; Pecoraro, V. L. A Mixed 3d-4f 14-Metallacrown-5 Complex That Displays Slow Magnetic Relaxation through Geometric Control of Magnetoanisotropy. *Inorg. Chem.* **2010**, *49*, 9104−9106. (c) Zaleski, C. M.; Depperman, E. C.; Kampf, J. W.; Kirk, M. L.; Pecoraro, V. L. Synthesis, Structure, and Magnetic Properties of a Large Lanthanide−Transition-Metal Single-Molecule Magnet. *Angew. Chem., Int. Ed.* **2004**, *43*, 3912−3914. (d) Deb, A.; Boron, T. T., III; Itou, M.; Sakurai, Y.; Mallah, T.; Pecoraro, V. L.; Penner-Hahn, J. E. Understanding Spin Structure in Metallacrown Single-Molecule Magnets using Magnetic Compton Scattering. *J. Am. Chem. Soc.* **2014**, *136*, 4889−4892. (e) Chow, C. Y.; Trivedi, E. R.; Pecoraro, V.; Zaleski, C. M. Heterometallic Mixed 3d-4f Metallacrowns: Structural Versatility, Luminescence, and Molecular Magnetism. *Comments Inorg. Chem.* **2015**, *35*, 214−253.
(28) Diethelm, R.; Miller, M. G.; Shibles, R.; Stewart, C. R. Effect of Salicylhydroxamic Acid on Respiration, Photosynthesis, and Peroxidase Activity in Various Plant Tissues. *Plant Cell Physiol.* **1990**, *31*, 179−185.
(29) (a) Vincent, J. B.; Chang, H.- R.; Folting, K.; Huffman, J. C.; Christou, G.; Hendrickson, D. N. Preparation and Physical Properties of Trinuclear Oxo-Centered Manganese Complexes of the General Formulation $[Mn_3O(O_2CR)_6L_3]^{0,+}$ (R = Me or Ph; L = a Neutral Donor Group) and the Crystal Structures of $[Mn_3O(O_2CMe)_6(pyr)_3](pyr)$ and $[Mn_3O(O_2CPh)_6(pyr)_2(H_2O)]\cdot 0.5MeCN$. *J. Am. Chem. Soc.* **1987**, *109*, 5703−5711. (b) Wemple, M. W.; Tsai, H.-L.; Wang, S.; Claude, J. P.; Streib, W. E.; Huffman, J. C.; Hendrickson, D. N.; Christou, G. Tetranuclear and Octanuclear Manganese Carboxylate Clusters: Preparation and Reactivity of $(NBu^n_4)[Mn_4O_2(O_2CPh)_9(H_2O)]$ and Synthesis of (NBu^n_4)-$[Mn_8O_4(O_2CPh)_{12}(Et_2mal)_2(H_2O)_2]$ with a "Linked-Butterfly" Structure. *Inorg. Chem.* **1996**, *35*, 6437−6449.
(30) *CrystalClear*; Rigaku/MSC Inc.: The Woodlands, TX, 2005.
(31) Sheldrick, G. M. *SHELXS-97, Program for Crystal Structure Solution*; University of Göttingen: Göttingen, Germany, 1997.
(32) Sheldrick, G. M. Crystal structure refinement with SHELXL. *Acta Crystallogr., Sect. C: Struct. Chem.* **2015**, *71*, 3−8.
(33) Kottke, T.; Stalke, D. Crystal handling at low temperatures. *J. Appl. Crystallogr.* **1993**, *26*, 615−619.
(34) *APEX2, Data Collection Software*, version 2.1-RC13; Bruker AXS: Delft, The Netherlands, 2006.
(35) *Cryopad, Remote Monitoring and Control*, version 1.451; Oxford Cryosystems: Oxford, U.K., 2006.
(36) *SAINT+, Data Integration Engine*, version 7.23a; Bruker AXS: Madison, WI, 1997−2005.
(37) Sheldrick, G. M. *SADABS, 2012/1, Bruker AXS Area Detector Scaling and Absorption Correction Program*; Bruker AXS: Madison, WI, 2012.
(38) Sheldrick, G. M. A short history of *SHELX*. *Acta Crystallogr., Sect. A: Found. Crystallogr.* **2008**, *64*, 112−122.
(39) Sheldrick, G. M. *SHELXT, Program for Crystal Structure Solution*, version 2014/3; University of Göttingen: Göttingen, Germany, 2014.
(40) Sheldrick, G. M. *SHELXL, Program for Crystal Structure Refinement*, version 2014; University of Göttingen: Göttingen, Germany, 2014.
(41) (a) Spek, A. L. PLATON, An Integrated Tool for the Analysis of the Results of a Single Crystal Structure Determination. *Acta Cryst. A* **1990**, *46*, C34. (b) Spek, A. L. Single-crystal structure validation with the program PLATON. *J. Appl. Crystallogr.* **2003**, *36*, 7−13. (c) van der Sluis, P.; Spek, A. L. BYPASS: an effective method for the refinement of crystal structures containing disordered solvent regions. *Acta Crystallogr., Sect. A: Found. Crystallogr.* **1990**, *46*, 194−201. (d) Bruno, I. J.; Cole, J. C.; Edgington, P. R.; Kessler, M. K.; Macrae, C. F.; McCabe, P.; Pearson, J.; Taylor, R. New software for searching the Cambridge Structural Database and visualizing crystal structures. *Acta Crystallogr., Sect. B: Struct. Sci.* **2002**, *58*, 389−397. (e) Bradenburg, K. *DIAMOND*, release 3.1f; Crystal Impact GbR: Bonn, Germany, 2008.
(42) Bain, G. A.; Berry, J. F. Diamagnetic Corrections and Pascal's Constants. *J. Chem. Educ.* **2008**, *85*, 532−536.
(43) (a) Brechin, E. K.; Soler, M.; Davidson, J.; Hendrickson, D. N.; Parsons, S.; Christou, G. A new class of single-molecule magnet: $[Mn_9O_7(OAc)_{11}(thme)(py)_3(H_2O)_2]$ with an $S = 17/2$ ground state. *Chem. Commun.* **2002**, 2252−2253. (b) Brechin, E. K.; Soler, M.; Christou, G.; Helliwell, M.; Teat, S. J.; Wernsdorfer, W. Dodecanuclear and octanuclear manganese rods. *Chem. Commun.* **2003**, 1276−1277.
(44) (a) Mazarakioti, E. C.; Poole, K. M.; Cunha-Silva, L.; Christou, G.; Stamatatos, T. C. A new family of Ln_7 clusters with an ideal D_{3h} metal-centered trigonal prismatic geometry, and SMM and photoluminescence behaviors. *Dalton Trans.* **2014**, *43*, 11456−11460. (b) Hooper, T. N.; Inglis, R.; Palacios, M. A.; Nichol, G. S.; Pitak, M. B.; Coles, S. J.; Lorusso, G.; Evangelisti, M.; Brechin, E. K. CO_2 as a reaction ingredient for the construction of metal cages: a carbonate-panelled $[Gd_6Cu_3]$ tridiminished icosahedron. *Chem. Commun.* **2014**, *50*, 3498−3500.
(45) (a) Khairy, E. M.; Shoukry, M. M.; Khalil, M. M.; Mohamed, M. M. A. Metal complexes of salicylhydroxamic acid: equilibrium studies and synthesis. *Transition Met. Chem.* **1996**, *21*, 176−180. (b) Hall, M. D.; Failes, T. W.; Hibbs, D. E.; Hambley, T. W. Structural Investigations of Palladium(II) and Platinum(II) Complexes of Salicylhydroxamic Acid. *Inorg. Chem.* **2002**, *41*, 1223−1228.
(46) Deacon, G. B.; Phillips, R. J. Relationships between the carbon-oxygen stretching frequencies of carboxylato complexes and the type of carboxylate coordination. *Coord. Chem. Rev.* **1980**, *33*, 227−250.
(47) Glazunov, V. P.; Mashkovsky, A. A.; Odinokov, S. E. Infared spectroscopic study of interionic hydrogen bonds in triethylammonium salts. *J. Chem. Soc., Faraday Trans. 2* **1979**, *75*, 629−635.
(48) (a) Langley, S. K.; Moubaraki, B.; Murray, K. S. Magnetic Properties of Hexanuclear Lanthanide(III) Clusters Incorporating a Central μ_6-Carbonate Ligand Derived from Atmospheric CO_2 Fixation. *Inorg. Chem.* **2012**, *51*, 3947−3949. (b) Dermitzaki, D.; Lorusso, G.; Raptopoulou, C. P.; Psycharis, V.; Escuer, A.; Evangelisti, M.; Perlepes, S. P.; Stamatatos, T. C. Molecular Nanoscale Magnetic Refrigerants: A Ferrimagnetic $\{Cu^{II}_{15}Gd^{III}_7\}$ Cagelike Cluster from the Use of Pyridine-2,6-dimethanol. *Inorg. Chem.* **2013**, *52*, 10235−10237.
(49) Liu, W.; Thorp, H. H. Bond Valence Sum Analysis of Metal-Ligand Bond Lengths in Metalloenzymes and Model Complexes. 2. Refined Distances and Other Enzymes. *Inorg. Chem.* **1993**, *32*, 4102−4105.
(50) For an excellent review on metallacrowns and their nomenclature, see: Pecoraro, V. L.; Stemmler, A. J.; Gibney, B. P.; Bodwin, J.; Kampf, J. W.; Wang, H. Metallacrowns: A New Class of Molecular Recognition Agents. In *Progress in Inorganic Chemistry*; Karlin, K. D., Ed.; John Wiley & Sons, Inc.: Hoboken, NJ, 1996; Vol. *45*, Chapter 2, p 83.
(51) Addison, A. W.; Rao, T. N.; Reedijk, J.; van Rijn, J.; Verschoor, G. C. Synthesis, structure, and spectroscopic properties of copper(II) compounds containing nitrogen-sulphur donor ligands; the crystal and molecular structure of aqua[1,7-bis(*N*-methylbenzimidazol-2′-yl)-2,6-dithiaheptane]copper(II) perchlorate. *J. Chem. Soc., Dalton Trans.* **1984**, 1349−1356.
(52) Zabrodsky, H.; Peleg, S.; Avnir, D. Continuous Symmetry Measures. 2. Symmetry Groups and the Tetrahedron. *J. Am. Chem. Soc.* **1993**, *115*, 8278−8289.
(53) Alvarez, S.; Alemany, P.; Casanova, D.; Cirera, J.; Llunell, M.; Avnir, D. Shape maps and polyhedral interconversion paths in transition metal chemistry. *Coord. Chem. Rev.* **2005**, *249*, 1693−1708.
(54) Siegbahn, P. E. M. Water oxidation mechanism in photosystem II, including oxidations, proton release pathways, O−O bond formation and O_2 release. *Biochim. Biophys. Acta, Bioenerg.* **2013**, *1827*, 1003−1019.

DOI: 10.1021/acs.inorgchem.7b01740
Inorg. Chem. 2017, 56, 10760−10774

(55) Kanady, J. S.; Lin, P.- H.; Carsch, K. M.; Nielsen, R. J.; Takase, M.K.; Goddard, W. A., III; Agapie, T. Toward Models for the Full Oxygen-Evolving Complex of Photosystem II by Ligand Coordination To Lower the Symmetry of the Mn_3CaO_4 Cubane: Demonstration That Electronic Effects Facilitate Binding a Fifth Metal. *J. Am. Chem. Soc.* **2014**, *136*, 14373−14376.
(56) Tsui, E. Y.; Tran, R.; Yano, J.; Agapie, T. Redox-inactive metals modulate the reduction potential in heterometallic manganese-oxido clusters. *Nat. Chem.* **2013**, *5*, 293−299.
(57) Nayak, S.; Nayek, H. P.; Dehnen, S.; Powell, A. K.; Reedijk, J. Trigonal propeller-shaped $[Mn^{III}_3M^{II}Na]$ complexes (M = Mn, Ca): structural and functional models for the dioxygen evolving centre of PSII. *Dalton Trans.* **2011**, *40*, 2699−2702.
(58) Mishra, A.; Wernsdorfer, W.; Abboud, K. A.; Christou, G. The first high oxidation state manganese-calcium cluster: relevance to the water oxidizing complex of photosynthesis. *Chem. Commun.* **2005**, 54−56.
(59) Kotzabasaki, V.; Siczek, M.; Lis, T.; Milios, C. J. The first heterometallic Mn-Ca cluster containing exclusively Mn(III) centers. *Inorg. Chem. Commun.* **2011**, *14*, 213−216.
(60) Hewitt, I. J.; Tang, J.- K.; Madhu, N. T.; Clerac, R.; Buth, G.; Anson, C. E.; Powell, A. K. A series of new structural models for the OEC in photosystem II. *Chem. Commun.* **2006**, 2650−2652.
(61) Fuller, R. O.; Koutsantonis, G. A.; Lozic, I.; Ogden, M. I.; Skelton, B. W. Manganese-calcium cluster supported by calixarenes. *Dalton Trans.* **2015**, *44*, 2132−2137.
(62) Li, N.; Wang, M.; Ma, C.- B.; Hu, M.- Q.; Zhou, R.- W.; Chen, H.; Chen, C.- N. Synthesis and characterization of a new 2D trimetallic Mn/Ca/Na complex. *Inorg. Chem. Commun.* **2010**, *13*, 730−732.
(63) Martin-Diaconescu, V.; Gennari, M.; Gerey, B.; Tsui, E.; Kanady, J.; Tran, R.; Pécaut, J.; Maganas, D.; Krewald, V.; Gouré, E.; Duboc, C.; Yano, J.; Agapie, T.; Collomb, M.- N.; DeBeer, S. Ca K-Edge XAS as a Probe of Calcium Centers in Complex Systems. *Inorg. Chem.* **2015**, *54*, 1283−1292.
(64) Wang, W.; Zhang, X.; Chen, F.; Ma, C.; Chen, C.; Liu, Q.; Liao, D.; Li, L. Homo- and hetero-metallic manganese citrate complexes: Syntheses, crystal structures and magnetic properties. *Polyhedron* **2005**, *24*, 1656−1668.
(65) Chen, C.; Zhang, C.; Dong, H.; Zhao, J. Artificial synthetic Mn^{IV}Ca-oxido complexes mimic the oxygen-evolving complex in photosystem II. *Dalton Trans.* **2015**, *44*, 4431−4435.
(66) Jerzykiewicz, L. B.; Utko, J.; Duczmal, M.; Sobota, P. Syntheses, structure, and properties of a manganese-calcium cluster containing a Mn_4Ca_2 core. *Dalton Trans.* **2007**, 825−826.
(67) Benniston, A. C.; Melnic, S.; Turta, C.; Arauzo, A. B.; Bartolomé, J.; Bartolomé, E.; Harrington, R. W.; Probert, M. R. Preparation and properties of a calcium(II)-based molecular chain decorated with manganese(II) butterfly-like complexes. *Dalton Trans.* **2014**, *43*, 13349−13357.
(68) Escriche-Tur, L.; Jover, J.; Font-Bardia, M.; Aullón, G.; Corbella, M. Magnetic Behavior of Heterometallic Wheels Having a $[Mn^{IV}_6M_2O_9]^{10+}$ Core with M = Ca^{2+} and Sr^{2+}. *Inorg. Chem.* **2015**, *54*, 11596−11605.
(69) For example, see: (a) Koumousi, E. S.; Raptopoulou, C. P.; Perlepes, S. P.; Escuer, A.; Stamatatos, T. C. Strong antiferromagnetic coupling in doubly *N,O* oximato-bridged dinuclear copper(II) complexes. *Polyhedron* **2010**, *29*, 204−211. (b) Pringouri, K. V.; Raptopoulou, C. P.; Escuer, A.; Stamatatos, T. C. Initial use of di-2-pyridyl ketone oxime in chromium carboxylate chemistry: Triangular $\{Cr^{III}_3(\mu_3\text{-}O)\}^{7+}$ compounds and unexpected formation of a carboxylate-free dichromium(II,II) complex. *Inorg. Chim. Acta* **2007**, *360*, 69−83. (c) Verani, C. N.; Bothe, E.; Burdinski, D.; Weyhermüller, T.; Flörke, U.; Chaudhuri, P. Synthesis, Structure, Electrochemistry, and Magnetism of $[Mn^{III}Mn^{III}]$, $[Mn^{III}Fe^{III}]$ and $[Fe^{III}Fe^{III}]$ Species. *Eur. J. Inorg. Chem.* **2001**, *2001*, 2161−2169. (d) Gass, I. A.; Milios, C. J.; Collins, A.; White, F. J.; Budd, L.; Parsons, S.; Murrie, M.; Perlepes, S. P.; Brechin, E. K. Polymetallic clusters of iron(III) with derivatised salicylaldoximes. *Dalton Trans.* **2008**, 2043−2053.
(70) Chilton, N. F.; Anderson, R. P.; Turner, L. D.; Soncini, A.; Murray, K. S. PHI: A Powerful New Program for the Analysis of Anisotropic Monomeric and Exchange-Coupled Polynuclear *d*- and *f*-block Complexes. *J. Comput. Chem.* **2013**, *34*, 1164−1175.
(71) (a) Beck, W. F.; Brudvig, G. W. Reactions of hydroxylamine with the electron-donor side of photosystem II. *Biochemistry* **1987**, *26*, 8285−8295. (b) Lin, C.; Brudvig, G. W. Chemical oxidation and reduction of the O_2-evolution center in Photosystem II. *Photosynth. Res.* **1993**, *38*, 441−448. (c) Riggs-Gelasco, P. J.; Mei, R.; Yocum, C. F.; Penner-Hahn, J. E. Reduced Derivatives of the Mn Cluster in the Oxygen-Evolving Complex of Photosystem II: An EXAFS Study. *J. Am. Chem. Soc.* **1996**, *118*, 2387−2399.
(72) (a) Sarrou, J.; Ioannidis, N.; Deligiannakis, Y.; Petrouleas, V. A Mn(II)−Mn(III) EPR Signal Arises from the Interaction of NO with the S_1 State of the Water-Oxidizing Complex of Photosystem II. *Biochemistry* **1998**, *37*, 3581−3587. (b) Ioannidis, N.; Sarrou, J.; Schansker, G.; Petrouleas, V. NO Reversibly Reduces the Water-Oxidizing Complex of Photosystem II through S_0 and S_{-1} to the State Characterized by the Mn(II)−Mn(III) Multiline EPR Signal. *Biochemistry* **1998**, *37*, 16445−16451.
(73) (a) Messinger, J.; Wacker, U.; Renger, G. Unusual Low Reactivity of the Water Oxidase in Redox State S_3 toward Exogenous Reductants. Analysis of the NH_2OH- and NH_2NH_2-Induced Modifications of Flash-Induced Oxygen Evolution in Isolated Spinach Thylakoids. *Biochemistry* **1991**, *30*, 7852−7862. (b) Bösing, P.; Willner, A.; Pape, T.; Hepp, A.; Mitzel, N. W. Structural diversity in bishydroxylamine complexes of gallium. *Dalton Trans.* **2008**, 2549−2556. (c) Kuntzleman, T.; Yocum, C. F. Reduction-Induced Inhibition and Mn(II) Release from the Photosystem II Oxygen-Evolving Complex by Hydroquinone or NH_2OH Are Consistent with a Mn(III)/Mn(III)/Mn(IV)/Mn(IV) Oxidation State for the Dark-Adapted Enzyme. *Biochemistry* **2005**, *44*, 2129−2142.
(74) Lampropoulos, C.; Thuijs, A. E.; Mitchell, K. J.; Abboud, K. A.; Christou, G. Manganese/Cerium Clusters Spanning a Range of Oxidation Levels and $CeMn_8$, Ce_2Mn_4, and Ce_6Mn_4 Nuclearities: Structural, Magnetic, and EPR Properties. *Inorg. Chem.* **2014**, *53*, 6805−6816.

DOI: 10.1021/acs.inorgchem.7b01740
Inorg. Chem. 2017, 56, 10760−10774